TÉCNICO LISBOA

Power Losses in Natural Gas and Hydrogen Transmission in the Portuguese High-pressure Network

Inês Alves Silvestre

Thesis to obtain the Master of Science Degree in

Mechanical Engineering

Supervisors: Dr. Rui Pedro da Costa Neto
Eng. Ricardo Manuel Santos Pastor

Examination Committee

Chairperson: Prof. António Luis Nobre Moreira
Supervisor: Dr. Rui Pedro da Costa Neto
Member of the Committee: Prof. Patrícia de Carvalho Baptista

November 2022

Declaration

I declare that this document is an original work of my own authorship and that it fulfills all the requirements of the Code of Conduct and Good Practices of the Universidade de Lisboa.

To my grandparents,

Acknowledgments

First and foremost, I would like to thank my supervisors, Professor Dr. Rui Costa Neto and Eng. Ricardo Pastor from R&D Nester, for their guidance and knowledge in the development of this work.

My greatest gratitude goes to my mother and father who provided me all the opportunities to complete this chapter of my life with all the success. I also thank all my family, my grandparents, cousin, and godparents, for your unconditional love and support. My accomplishments are yours too.

To my boyfriend, thank you for all the love, support, patience, and help. I am beyond grateful to complete this journey with you, and for us to become Mechanical Engineers together. You brightened all this adventure.

Finally, I am deeply grateful for my closest friends for all the memories created in these five years and for those yet to come. I am proud of all of you. This is only the beginning.

Resumo

Atualmente, juntamente com a emergência climática, a escassez de energia é um desafio mundial. Por isso, poupar energia é essencial, por exemplo, melhorando eficiências energéticas. O transporte de gás natural dentro de gasodutos tem perdas de potência associadas. Neste contexto, esta Dissertação centra-se no desenvolvimento de uma ferramenta computacional representativa da rede portuguesa de gás em alta pressão que abastece os consumidores industriais portugueses. Esta ferramenta calcula o caudal mássico exigido por cada cliente industrial e as perdas de potência associadas ao fornecimento. Vários cenários de abastecimento são definidos e verifica-se que abastecer a indústria portuguesa desde Sines tem perdas de potência de 4.21%. A exportação para Espanha tem menores perdas de potência quando dividido entre Campo Maior e Valença. O enchimento do Armazenamento Subterrâneo de Gás do Carriço tem maiores perdas de potência, mas é vantajoso utilizar o gás armazenado para abastecer a indústria. Quando hidrogénio é adicionado na mistura, as perdas de potência aumentam e uma correlação linear é desenvolvida para misturas com 0 a 20% de hidrogénio em volume. Uma avaliação económica é conduzida para produzir hidrogénio, o Custo Nivelado de Hidrogénio, Valor Atual Líquido, Taxa Interna de Retorno e Período de Retorno são 4.99 €/kg, 242.79 M€, 21% e 5 anos, respetivamente. Para todos os cenários, o Valor Atual Líquido é positivo, sendo mais sensível ao preço do hidrogénio e eletricidade. O impacto económico na indústria é altamente sensível aos preços considerados.

Palavras-chave: Perda de Potência, Gasodutos, Gás Natural, Hidrogénio, Rede Nacional de Transmissão de Gás Natural, Análise Económica

Abstract

Nowadays, along with climate emergency, energy shortage is a challenge being faced worldwide. For such, energy savings play an essential role, for example, by improving energy efficiencies. Transporting natural gas inside pipelines has associated power losses. In this context, the Dissertation focuses on developing a computational tool representing the Portuguese high-pressure gas network supplying Portuguese industrial consumers. This tool computes the mass flow rate required by each industry and the power losses associated with its supply. Several scenarios are defined and supplying the Portuguese industry from Sines has a power loss of 4.21%. The exportation to Spain has fewer power losses when divided through Campo Maior and Valença. Filling Carriço Underground Storage has higher power losses associated, but it is advantageous to use the gas stored to later supply the industry. Power losses increase when hydrogen is added in the mixture, and a linear correlation is developed for 0 to 20% of hydrogen in volume. An economic assessment is conducted for producing hydrogen, and Levelised Cost of Hydrogen, Net Present Value, Internal Rate of Return, and Payback Period are 4.99 €/kg, 242.79 M€, 21%, and 5 years, respectively. The Net Present Value is positive for all scenarios, being most sensitive to hydrogen selling and electricity prices. The economic impact on the industry is highly sensitive to the prices considered.

Keywords: Power Loss, Pipeline, Natural Gas, Hydrogen, Portuguese Natural Gas Transmission Network, Economic Assessment

Contents

List of Tables

List of Figures

Nomenclature

Greek symbols

Δ	Variable variation
κ	Thermal conductivity coefficient
μ	Dynamic viscosity
Φ	Energy flow
ρ	Density
ε	Internal surface absolute roughness

Roman symbols

C_p	Specific heat
D	Diameter
F	Electricity costs
f	Friction factor
h	Heat transfer coefficient; Specific enthalpy
I	CAPEX
L	Length
M	Mass; Mass molar
$\dot{m}$	Mass flow rate
n	Project lifetime
Nu	Nusselt number
O	OPEX
p	Pressure
Pr	Prandtl

Q	Volumetric flow rate
q	Heat flow rate
R	Specific gas constant
r	Rate of return on investment
Re	Reynolds number
S	Cross-sectional area
T	Temperature
t	Time
U	Internal energy
Z	Compressibility factor

Subscripts

0	Year 0
avg	Average
cond	Conductive
conv	Convective
eqv	Equivalent
hyd	Hydraulic
insul	Insulation
in	Inlet
I	Internal node
mix	Mixture
mol	Molar
out	Outlet
surf	Surface
sur	Surroundings
turb	Turbulent
t	Year t
vol	Volume

Superscripts

n Lifetime of the project

t Year t

Acronyms

AEL Alkaline electrolysis

bcm Billion cubic meters

C2H Coal-to-hydrogen

C2HCCS Coal-to-hydrogen with carbon capture and storage

CAPEX Capital expenditures

CF Cash flow

CPA Organic carboxylate polymer

DRA Drag reduction agent

EGIG European Gas Pipeline Incident Data Group

ERSE Energy Services Regulatory Authority

FC Fuel cell

FCEV Fuel cell vehicle

GDE Gas diffusion electrode

GHG Greenhouse gases

GRMS Gas regulation and metering stations

HHV Higher heating value

IPCC Intergovernmental Panel on Climate Change

IRR Internal Rate of Return

LCOH Levelised Cost of Hydrogen

LHV Lower heating value

LNG Liquified natural gas

LPG Liquified petroleum gas

MIBGAS Iberian Natural Gas Market

NG Natural gas

NPV Net Present Value

NRA National Regulatory Authority

OPEX Operational expenditures

PBP Payback Period

PDE Partial differential equation

PEMEL Proton exchange electrolysis

PIGS Pipeline intervention gadgets

PLC Programmable logic controllers

RNTGN Portuguese Natural Gas Transmission Network

SCADA Supervisory control and data acquisition

SOEL Solid Oxide electrolysis

Chapter 1

Introduction

Chapter 1 is divided into several sections, such as ”Motivation”, ”Description and Overview”, ”Literature Review”, ”Objectives”, and ”Dissertation Outline”. Firstly, Section 1.1 explains the motivation behind this Dissertation. Afterwards, Section 1.2 regards Natural Gas (NG) and Hydrogen ($\mathrm{H_2}$). Finally, the objectives of the Dissertation are enumerated in Section 1.4 and the Dissertation is outlined in Section 1.5.

1.1 Motivation

Nowadays, climate emergency is one of the most concerning challenges being faced worldwide. The greenhouse gases (GHG) emissions to the atmosphere, including the well-known carbon dioxide ($\mathrm{CO_2}$), allied with energy dependence on fossil fuels have aggravated this environmental crisis. Urgent measures must be implemented to reverse the decaying situation that all nations find themselves in. One example is the Paris Agreement presented by the United Nations in 2015 and signed by 196 countries [1]. The Paris Agreement stated that sustainable technologies should be developed with the aim of limiting the increase of temperature below $2^{\circ}\mathrm{C}$ compared to pre-industrial levels, while attempting to go even further to $1.5^{\circ}\mathrm{C}$. Furthermore, according to the Intergovernmental Panel on Climate Change (IPCC), the world needs to be net-zero by 2050 to comply with the increase of $1.5^{\circ}\mathrm{C}$ [2]. Another measure is the creation of the Roadmap 2050 [3] by the European Council, which has the objective to decrease the GHG emission to at least 80% below 1990 levels by 2050, as well as the initiatives European Green Deal [4] and Fit for 55 [5].

Along with the climate emergency, another challenge being faced nowadays is the energy shortage [6]. The supply of NG, coal and other energy sources is insufficient to satisfy demand, and, as a result, the planet is undergoing through an energy crisis. This problem has been aggravated by the interruption of the gas supply from Russia, and it will become even worsened by the eventual run-out of reserves [7]. The European Comission presented the REPowerEU Plan [8] due to both the necessity to address the climate crisis and Europe’s dependency on Russian fossil fuels, which make it urgent for Europe to reform its energy system. The most effective method to address the present energy shortages is to

save energy rather than generate more energy [9]. In this context, energy saving means decreasing the energy consumption of a unit product, which is to improve energy efficiency.

The role of alternative fuels and technologies, which are intended to assist the energy transition, is uncertain, as is the future low-carbon pathway. Another promising concept through a more sustainable path is the usage of $\mathrm{H_2}$ as an alternative fuel. This application has the potential to decrease GHG emissions when it is produced from renewable sources – green hydrogen. In this framework, Portugal has developed the National Strategy for Hydrogen in 2020 [10], with a target of incorporating hydrogen to promote the decarbonisation of the Portuguese NG network, and consequently, to contribute to the decarbonisation of the industrial and transport sectors while granting energy security supply.

1.2 Description and Overview

Section 1.2 is about the description and overview of both NG and $\mathrm{H_2}$. The NG is regarded in Subsection 1.2.1, where the global and Portuguese context are described, followed by a brief introduction about the NG establishment in Portugal, the characterisation of the Portuguese Natural Gas Transmission Network (RNTGN), some considerations about pipeline manufacturing, operation and security, the Sines Liquified Natural Gas (LNG) Terminal, and the Carriço Underground Storage. Subsection 1.2.2 describes the $\mathrm{H_2}$, specifically its applications, production, and types of electrolysers.

1.2.1 Natural Gas

NG is a fossil energy source composed of a mixture of gases, in which methane ($\mathrm{CH_4}$) is its main component with a percentage between 70-90% in the mixture [11]. It also contains smaller quantities of NG liquids – hydrocarbon gas liquids –, and nonhydrocarbon gases, such as carbon dioxide ($\mathrm{CO_2}$) and water ($\mathrm{H_2O}$) vapour. This type of fossil energy source is a result of the remains of plant and animal matter being built up in thick layers on the Earth's surface over millions to hundreds of millions of years. Over time, these layers have been exposed to intense heat and pressure, which transformed these materials into coal, some into petroleum, and some into NG. NG may be found in sedimentary basins, accessible through a drilled hole or well, and is usually extracted by vertical drilling. These wells can be either on-land or off-shore. In the case of on-land wells, they enable the capture of NG from deposits in continental subsoils, whereas off-shore wells allow the extraction of NG from subsea deposits.

Although its existence has been known since early history, its economic application is considered relatively recent. For instance, on Mount Parnassus in ancient Greece, the famed Oracle at Delphi was established in $1000\ \mathrm{B.C.}$, where NG seeped from the ground in a flame. Around $500\ \mathrm{B.C.}$, the Chinese began using rudimentary bamboo "pipelines" for carrying gas that had seeped to the surface to boil seawater to produce drinkable water. Native Americans in the United States discovered NG properties, which they used to ignite the gases that seeped into and surrounded Lake Erie. Around 1626, French explorers observed and learned this technique. Afterwards, NG was first commercialized in Britain, where the British employed coal-fired NG to power lighthouses and roadways around 1785. During most

of the 19^{th} century, NG was almost solely utilized as a source of light, however, in 1885, Robert Bunsen's creation of the Bunsen burner brought up a world of new possibilities for NG utilization. After effective pipelines were developed in the 20^{th} century, NG began to be used for house heating and cooking, equipment such as water heaters and oven ranges, manufacturing and processing plants, and boilers to generate electricity.

Nowadays, NG has been considered one of the most important types of fuel in the world's energy supply, being the most consumed worldwide along with coal and oil [11]. The NG relevance has been sustained both by its versatility and flexibility and by being the cleanest-burning hydrocarbon. In fact, its flexibility has allowed NG to become a reliable partner for renewable energy sources, assisting in matching the supply and demand for wind, solar, and hydroelectricity. Moreover, when NG is burned to generate electricity, it emits around half the CO_2 and one-tenth the air pollutants that coal does [12]. Therefore, the replacement of coal by NG has shown significant potential in minimizing near-term CO_2 emissions and air pollution. Despite all these advantages, the exclusive usage of NG is no longer viable since the ultimate objective is to cease the emission of pollutant substances and to suspend the dependency on non-renewable energy sources, which only aggravates the difficulties related to energy shortages. However, the NG cessation must be effectuated continuously to slowly decarbonise the economies since the global market is still immensely dependent on NG, as can be verified next.

Global Context

In 2019, global NG consumption amounted to a total of 4021 billion cubic meters (bcm) [13]. The NG consumption *per capita* in 2019 [14] is illustrated in Figure 1.1. As can be observed, Portugal presented a consumption in 2019 of about $20 - 40$ GJ *per capita*, significantly lower than some countries such as Canada, United States, Russia, Australia, United Kingdom, Italy, *etc*.

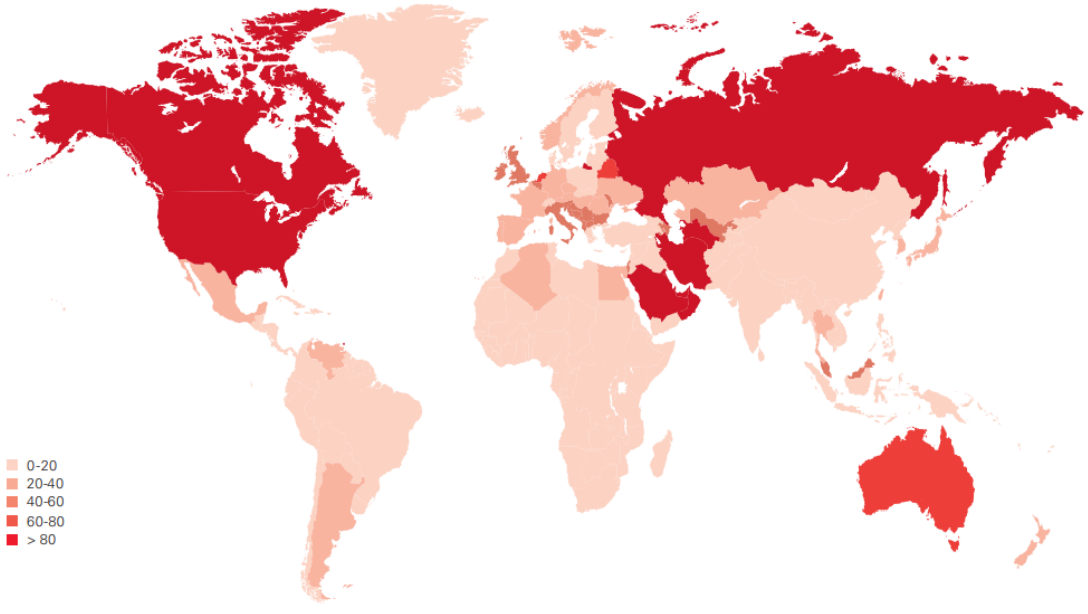

Figure 1.1: NG consumption *per capita* [GJ], from [14].

The major trade movements of NG in 2019 [14] are represented in Figure 1.2, in which the worldwide trade flow (in bcm) of both pipeline gas and LNG are depicted. By analysing Figure 1.2, the trade flow of LNG evidence a clear dominance over the pipeline gas trade flow in the year 2019.

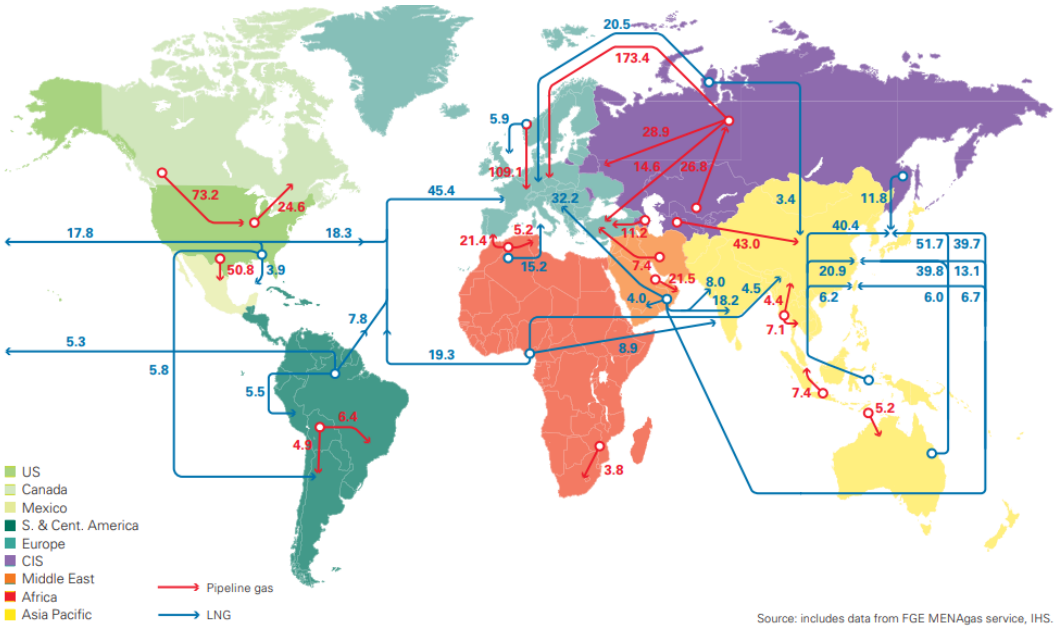

Figure 1.2: Major trade flow movements of 2019 [bcm] using pipeline gas (red) and LNG (blue), from [14].

Concerning the supply, gas production accounted for $4115\ \mathrm{bcm}$ [13], surpassing the global demand. Particularly, the United States accounted for over two-thirds of net worldwide growth and a significant expansion in Australia and China also helped to enhance the supply. Most of the gas output increase in 2019 was utilized to feed additional LNG exports. Therefore, LNG exports increased, led by record increases from the United States and Russia, as well as sustained growth from Australia. In terms of LNG imports, practically all new supply was directed to Europe. European LNG imports increased by 49 bcm, representing a historic 68% increment. Growth was widespread, with the United Kingdom, France, and Spain contributing the most. Due to the general rapid growth of LNG, the overall inter-regional gas trade also increased by 4.9%. Despite a drop in pipeline trade, pipeline imports into Europe from Russia and North Africa were partially driven out by the abundance of LNG supplies. At the present time, it should be denoted that the dynamic of these trade flow movements is strongly affected by the interruption of gas supply from Russia, influencing the overall panorama.

Portuguese Context

The Portuguese gas supply infrastructure is completely dependent on imported gas since Portugal does not have any domestic gas fields of its own being explored. Thus, the imported gas can be supplied through two alternatives. The first option is the supply of gas in the form of LNG which is delivered by gas tankers in the LNG terminal of Sines, located in the southwest of the country. Another alternative is in the form of high-pressure gas transported through the Euro-Maghreb pipeline, which connects North Africa with Central Europe. There are three major groups of NG consumers in Portugal: combined-cycle

gas power plants, industrial consumers, and domestic consumers. In terms of provisions about the NG demand, the consumption supplied by the distribution network to domestic consumers is relatively stable. Meanwhile, the consumption supplied by the high-pressure transmission network to industries is related to a reduced number of consumers, being greatly influenced by external factors, such as economic factors. Finally, the electric energy production in combined-cycle gas power plants is strongly affected by the electricity market dynamics and renewable energy production, particularly wind and hydropower plants. In this sense, the overall NG demand in Portugal is mainly dictated by the consumption of the industrial sector as well as combined-cycle gas power plants, despite most of the consumers being domestic.

Regarding the annual NG consumption in 2019, this value is estimated at $66.8\ \mathrm{TWh}$ [15]. Figure 1.3 illustrates a decrease of 22% in national consumption between 2011 and 2014. This abrupt decrease may be explained due to the reduction in the consumption of gas power plants that resulted from the proliferation of renewable energy sources, such as wind and the availability of hydro resources. However, this trend inverts in 2015 as the consumption of combined-cycle gas power plants increased, until 2017. Finally, the data from 2017 to 2019 evidence a stabilisation of the demand for NG.

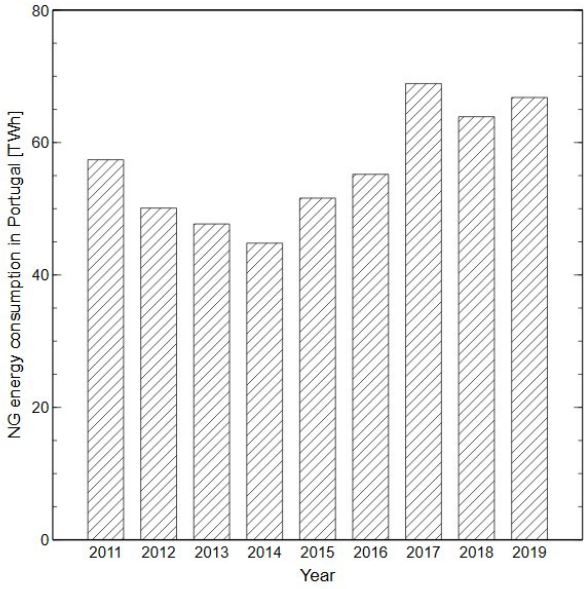

Figure 1.3: NG energy consumption in Portugal [TWh] in each year, adapted from [15].

The LNG Terminal at Sines received $62.7\ \mathrm{TWh}$ in 2019, accounting for 91% of the whole supply whereas the interconnections with Spain (Campo Maior and Valença do Minho) totalled the remaining 9%, as can be observed in Figure 1.4. Contrastingly, the exportations through these interconnections are estimated at around $0.7\ \mathrm{TWh}$. Furthermore, 64 ship unloading operations were registered at the Sines terminal, denoting an increase of 16 more operations when compared to 2018. Particularly, the gas entering Sines derived 57% from Nigeria, while 25% came from the United States. Finally, this terminal injected $61.6\ \mathrm{TWh}$ into the grid, which is 48% more than the previous year, and it filled 6620 LNG tanker trucks with $1.9\ \mathrm{TWh}$, including $0.4\ \mathrm{TWh}$ intended for the Madeira Autonomous Region. In terms of imports through interconnections, this value amounted to $6.0\ \mathrm{TWh}$, which has been continuously

decreasing throughout the past three years. The Carriço Underground Gas Storage moved 10% more gas than in 2018, accounting for 6.7 TWh. Overall, the RNTGN transported approximately 71.1 TWh in 2019, supplying for distribution grids, direct high-pressure consumers, the Carriço Underground Gas Storage, and the flow in the interconnections.

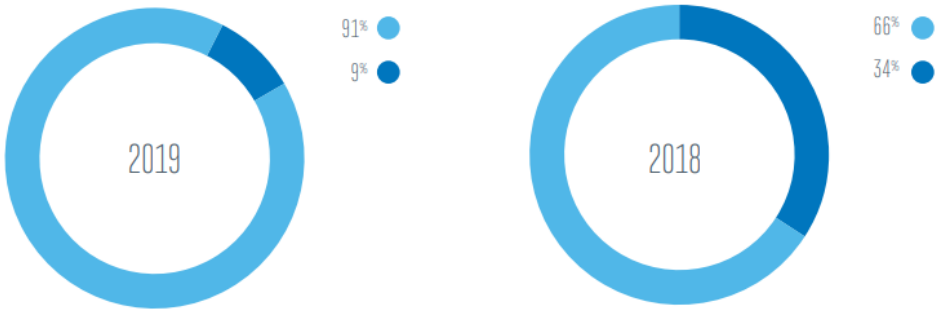

Figure 1.4: Pipeline NG (dark blue) and LNG (light blue) input share in Portugal's NG import, from [16].

Brief introduction about the NG establishment in Portugal

The introduction of NG in Portugal was a fundamental contribution to the country's development, by diversifying its energy matrix as well as instigating a new energetic alternative for the productive sectors and consumers. To this extent, Portugal was able to increase the potentiality of its industry due to promoting social development and improving the security of the energy supply. Some introductory proposals to establish NG in Portugal emerged in the decade of 1980. Subsequently, the first distribution concessions in urban areas were built in the decade of 1990. In 1993, Transgás - Sociedade Portuguesa de Fornecimento de Gás Natural, S.A. (currently known as Galp Gás Natural, S.A.) was established and the NG import, transport and storage, and concession contract were signed between the Portuguese State and this new entity. Followingly, Transgás started the construction of the high-pressure pipeline between Setúbal and Braga in 1994. Also, the contract for the selling of NG for electricity generation was signed at the Tapada do Outeiro Combined-Cycle Gas Power Plant in Gondomar. In 1997, NG started being distributed, and from 1998 on, pipeline infrastructures were constructed in several locations (Coimbra-Mangualde, Portalegre-Guarda, Sines-Setúbal). Subsequently, the preparatory work for the Sines LNG terminal began with the preparation of the ground in 2000. The first unload operations at the LNG terminal in Sines occurred in 2003. Afterwards, the combined-cycle gas power plant of Carregado was inaugurated in 2004 and Galp Energia's General Meeting approved the unbundling process for the transfer of ownership of regulated NG assets to REN - Redes Energéticas Nacionais, S.A. in 2006. In the same year, a NG storage project in Pombal, named Carriço Underground Storage, was inaugurated, and Energy Services Regulatory Authority (ERSE) approved the NG sector regulation. Finally, the Iberian Natural Gas Market (MIBGAS) was created in 2008. The establishment and development of MIBGAS and the resulting integration of the Portuguese and Spanish gas networks were beneficial for consumers and traders of both countries. MIBGAS has the objective of ensuring access to all agents under the same circumstances of fair treatment, transparency, and objectivity. Furthermore, MIBGAS aims to increase

supply security by integrating markets and coordinating both systems in the NG sector, as well as by strengthening interconnections. Also, it pursues to increase the competition, which may reflect in a wider market with a larger set of participants. Another goal is to simplify and harmonize the regulatory framework of both countries as well as to encourage the efficiency of regulated and liberalized activities.

Portuguese Natural Gas Transmission Network

REN Gasodutos S.A. is the responsible entity for the operation of the RNTGN. By owning the concession of the high-pressure NG transmission, this entity manages both the national NG system and NG transmission infrastructure, ensuring the security and resilience of the NG supply. All these operations are verified and audited by the National Regulatory Authority (NRA) – ERSE –, which is governed by the framework law of regulatory authorities, and it aims to regulate electricity, NG, and Liquefied Petroleum Gas (LPG) sectors in all their categories, throughout the Portuguese territory.

The RNTGN can receive NG through the Spanish border, from the Carriço Underground Storage (concession of REN Armazenagem S.A.), or through the regasification LNG Terminal in Sines (concession of REN Atlântico S.A.). Subsequently, RNTGN supplies NG it to distribution network operators and high-pressure consumers. High-pressure NG flows inside the gaseous pipelines sometimes for thousands of kilometers. However, before entering these pipelines, this gas must be compressed in a compression station to attain this higher pressure (approximately $84\ \mathrm{bar}$). The NG from high-pressure pipelines is transmitted to medium-pressure branches at the distribution level through the usage of gas regulation and metering stations (GRMS). This medium-pressure and low-pressure network branching are part of the distribution networks, whose responsibility is to deliver NG to its end-users.

Pipeline Manufacturing

NG is often transported in pipelines, which are large pipes composed of steel with more than 10% of chromium (Cr) buried at a 1-meter depth [17]. Regarding pipe manufacturing, a steel coil undergoes a submerged arc welding process, followed by a low-density polyethylene coating. Subsequently, the manufactured pipes are subjected to testing to verify their integrity, and the inside of the pipes are engraved with related information. The pipes are then shipped or trucked to their final location. Afterwards, the lane opening is effectuated in the desired location, and the piping is properly aligned. The bending machine starts operating as well as the welding process to assemble several segments of piping. The ditch is excavated, and the piping is placed inside the excavation. At last, a test is performed on the pipeline's coating to verify its reliability, after which is prepared to be utilized. The construction and assembly of the piping infrastructure must comply with both *EN 1594/2009 Gas Supply Systems: Pipelines for Maximum Operating Pressure over 16 bar for Steel Systems* and *ISO 13623/2017 Petroleum and Natural Gas Industries Pipelines Transportation Systems*. The documents of these standardization codes describe the functional requirements of pipeline systems, providing a basis for their safe design, construction, testing, operation, maintenance, and abandonment.

Operation and Security

A supervisory control and data acquisition (SCADA) system based on remote programmable logic controllers (PLC) is utilized to monitor pipelines and stations, which collects local data, such as pressure, temperature, flow rate, odorization, and position of sectioning valves. This system communicates with the dispatch centre, being able to close the station valves in the scenario of system damage. It is also connected to software that monitors the conditions of the gas pipeline to detect possible leaks. Another relevant technology is the In-Line Inspection, which consists of periodically examining the pipelines using pipeline intervention gadgets (PIGS). This intelligent tool travels inside the pipe driven by the gas itself, reporting any detected defect in the pipe structure, for example, cracks in welds, state of coating, or other deformations. The collected data is then analysed by software to assess the defect evolution and to decide the most suitable reparation.

The several segments of piping are classified into categories with different safety factors and compulsory distances between sectioning valves. The classification accounts for local considerations, such as population density, environment, buildings and constructions, as well as, road and rail traffic intensity. Moreover, this categorization is sustained through statistics about operator risk analysis provided by the European Gas Pipeline Incident Data Group (EGIG). Essentially, EGIG is a cooperation between gas transmission system operators whose objective is to collect data on unintentional releases of gas from their pipelines, ultimately attempting to increase the safety of their systems. This database only includes incidents with an unintentional gas release in on-land gas transmission steel pipelines with a design pressure higher than $15\ \mathrm{bar}$, excluding incidents related to equipment (for example, valves and compressors) or other parts rather than the pipeline itself.

Figure 1.5 showcases the number of incidents *per* year, evidencing an overall decreasing trend through the years. Furthermore, Figure 1.6 presents the incident distribution *per* cause between 2010 and 2019, in which is denoted that corrosion and external interference incidents are the major causes of accidents. The fact of external interferences are one of the main risks of buried pipelines justifies the increase in the safety factor and the number of sectioning valves with aggravation of danger.

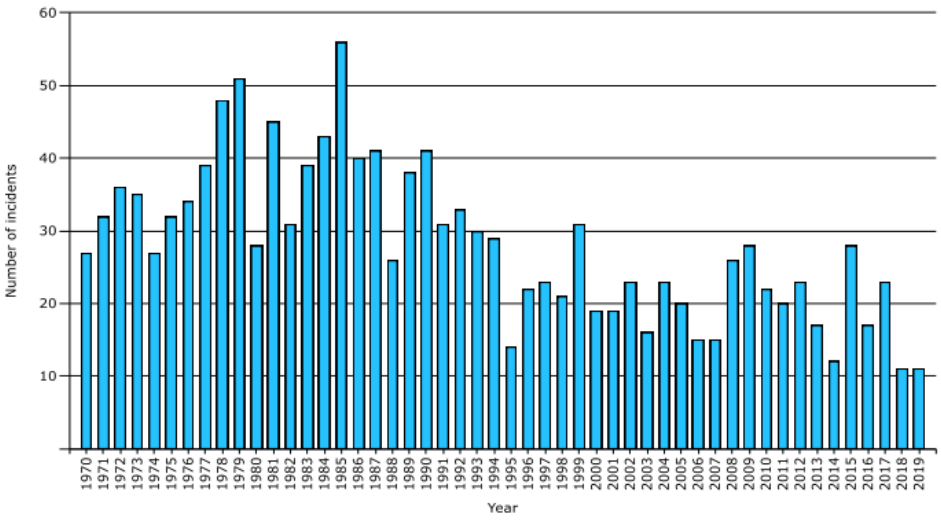

Figure 1.5: Number of incidents in NG transmission through pipelines *per* year, from [18].

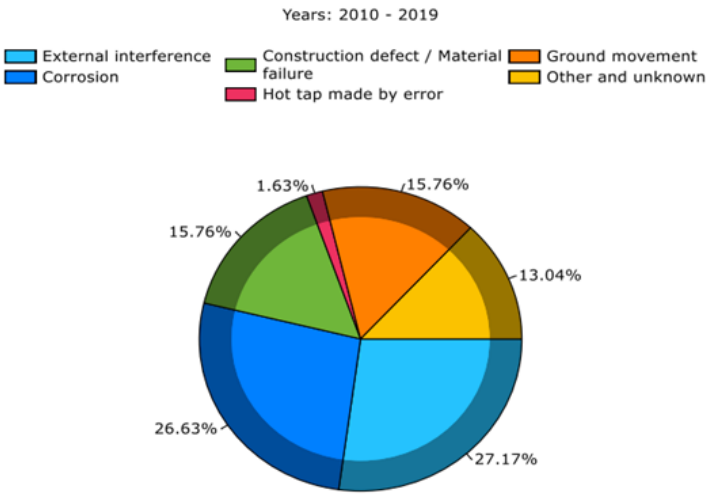

Figure 1.6: Pipeline transmission incident distribution *per* cause, from [18].

Sines LNG Terminal

LNG is NG that has been cooled to $-162°\mathrm{C}$, attaining a liquid state. This liquefaction process reduces its volume about 600 times compared to the volume in the gaseous state in a NG pipeline [19]. In fact, this decrease in volume provides easier, safer, and more economical transmission and storage as well as contribute to transporting NG to locations where pipelines do not exist [20]. The operation starts with the delivery of NG via pipeline to LNG export facilities, where it is liquefied to be transported by ocean-going LNG ships or tankers. The majority of LNG is transported by tankers – LNG carriers – in massive, onboard super-cooled tanks. Alternatively, LNG may also be carried in smaller ISO-compliant containers that can be carried on ships and trucks. LNG is offloaded from ships at import terminals. Followingly, it is stored inside cryogenic storage tanks, before being returned to its gaseous state at regasification plants. Afterwards, the NG is piped to NG-fired power plants, industrial facilities, and residential and commercial users.

The Portuguese LNG Terminal is situated in the industrial region of Sines, located on the Portuguese Atlantic coast. This terminal station has extreme importance within the Portuguese context since it constitutes a viable alternative to on-land piping. Particularly, the installation of the Sines terminal is composed of 3 LNG storage tanks with a total storage capacity of $390217\ \mathrm{m}^3$ as well as a berth for receiving and unloading tankers with a capacity from 40000 to $216000\ \mathrm{m}^3$ and an unloading time of about $20\ \mathrm{hours}$. It is also equipped with a regasification facility constituted of 7 open-rack vaporizers, and it has 3 bays for filling tanker trucks to supply autonomous regasification units located across the country. Furthermore, the LNG terminal has a nominal emission capacity of $900000\ \mathrm{m}^3/\mathrm{hour}$, a maximum capacity of $1350000\ \mathrm{m}^3/\mathrm{hour}$, and a daily loading capacity of 36 tanker trucks [21]. The terminal is connected to the RNTGN.

Carriço Underground Gas Storage

NG can be stored underground in various geological structures, aiming to store strategic gas reserves, maintain energy prices stable, as well as, balance supply and demand since there are repeatedly seasonal and daily fluctuations in demand. Particularly, there are three common types of underground storage, such as depleted gas reservoirs, aquifers, and salt caverns. All these storage facilities are safe solutions with low space requirements and reasonable costs when compared with above-ground storage tanks [22]. Large quantities of a wide variety of gases such as NG, compressed air, hydrogen ($\mathrm{H_2}$), and nitrogen ($\mathrm{N_2}$), as well as liquid hydrocarbons such as crude oil, gasoline, ethylene ($\mathrm{C_2H_4}$), propylene ($\mathrm{C_3H_6}$) can be stored inside them [23].

The Carriço Underground Gas Storage is the first project of this type to be established in the Portuguese territory, storing NG inside salt caverns in the Monte Real salt dome located in Pombal, as indicated in Figure 1.7. The storage caverns are part of an underground geological structure primarily constituted by rock salt beds with intercalated non-salt horizons like claystone, anhydrite, and dolomite. In terms of the cavern's construction, the decision of the location to construct a new well is dependent on a set of factors including targeted deposit, infrastructure, accessibility, environmental regulations, *etc*.

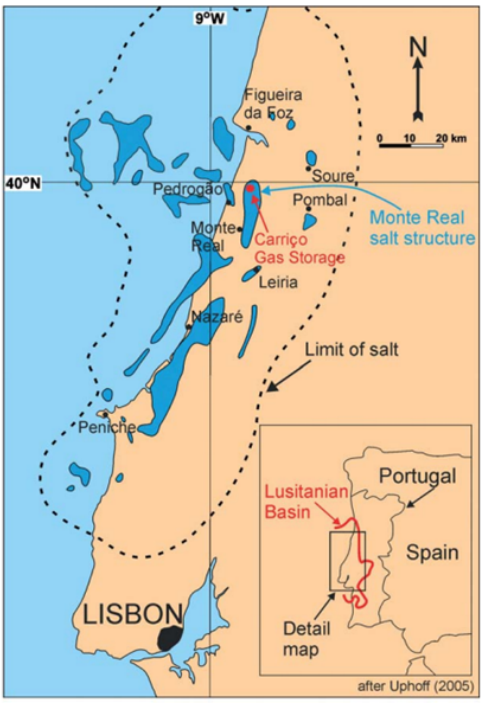

Figure 1.7: Monte Real salt structure within the Lusitanian Basin, from [23].

The Carriço complex is constituted of 6 caverns with depths ranging from 900 to 1500 meters, as represented in Figure 1.8, accounting for a total geometrical volume of 3.21 million $\mathrm{m^3}$. Overall, these caverns can store approximately 333.4 million $\mathrm{m^3}$ of working gas.

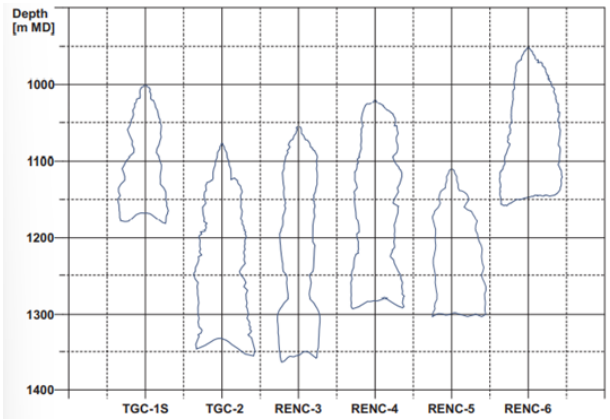

Figure 1.8: Shape and depth of the 6 caverns of Carriço Underground Gas Storage, from [23].

1.2.2 Hydrogen

One of the most abundant elements in nature is H_2 (10^{th} most abundant on Earth's crust), which is present in many other substances such as H_2O, alcohol, and hydrocarbons, and it can also be found in biomass from animals or plants. H_2 is an energy carrier and it allows to carry or store energy. H_2 can be used in a wide variety of industrial applications, including fertilizers, petroleum refining, petrochemical, and chemical industries. Regarding H_2 production, different processes can be used to produce H_2 [24]. Heat and chemical reactions are used in thermochemical processes to extract H_2 from organic materials such as fossil fuels and biomass, as well as from H_2O. Using electrolysis, H_2O can also be split into H_2 and oxygen (O_2). Through biological processes, microorganisms such as bacteria and algae can also produce H_2. Particularly, the H_2 produced from fossil fuels is denominated grey H_2, and the one produced from renewable sources is known as green H_2. The various H_2 production methods are summarized in the scheme of Figure 1.9.

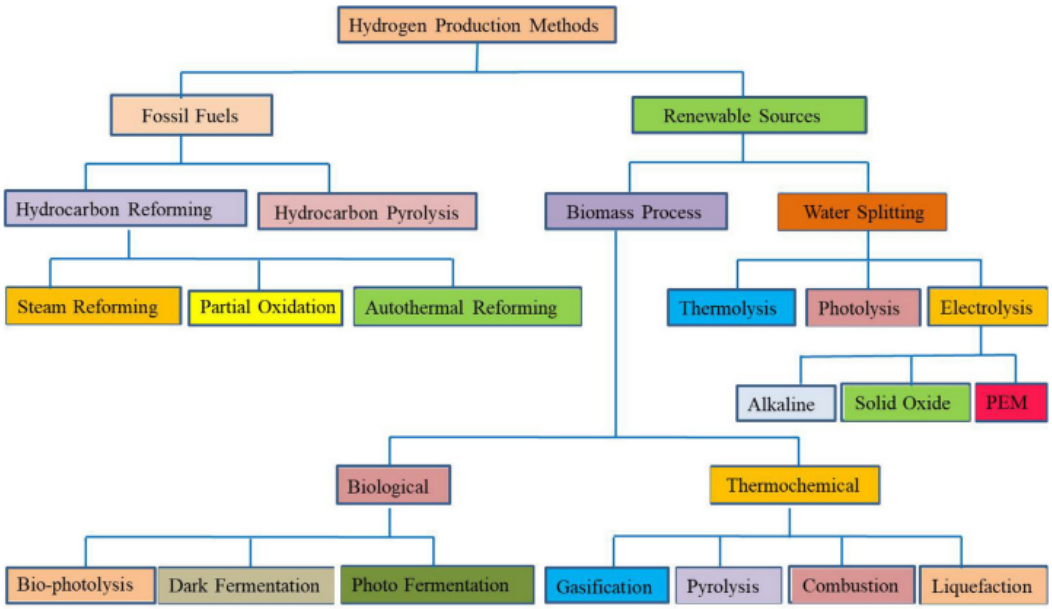

Figure 1.9: Methods for producing H_2, either by fossil fuels or renewable energy sources, from [25].

Electrolysis can be a prospective process for producing green H_2 if produced from renewable resources. It consists of the splitting of H_2O molecule into H_2 and O_2 using electricity, and the respective main chemical reaction is presented in Equation (1.1).

$$H_2O \Longrightarrow 2H_2 + O_2 \tag{1.1}$$

This reaction occurs in a so-called electrolyser. There are several types of electrolysers commercially available, depending on their size and function, and the most frequently used include alkaline electrolysis (AEL), proton exchange membrane electrolysis (PEMEL), and solid oxide electrolysis (SOEL). To exemplify, the AEL produces H_2 in assembled cells composed of an anode, a cathode, and a membrane. The design of this type of electrolyser is represented in Figure 1.10. The principle of operation of AEL is the movement of hydroxide ions (OH^-) through the electrolyte from the cathode to the anode, generating H_2 on the cathode side and O_2 on the anode side. The correspondent chemical reactions are presented in Equation (1.2) and (1.3), for the anode and cathode, respectively. Also, this type of electrolyser uses a liquid electrolyte solution of potassium hydroxide (KOH) or sodium hydroxide ($NaOH$).

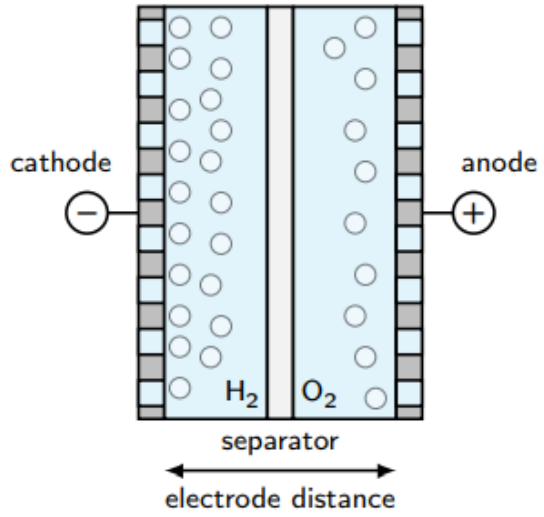

Figure 1.10: Cell design of an AEL, from [26].

$$\text{Anode} : H_2O \Longrightarrow 2H^+ + \frac{1}{2}O_2 + 2e^- \tag{1.2}$$

$$\text{Cathode} : H_2O + 2e^- \Longrightarrow H_2 \tag{1.3}$$

Nowadays, green H_2 is attracting a lot of interest due to the obvious growing awareness about climate change and emissions from conventional energy sources. As a result, H_2 has enormous potential to help to decarbonise the energy sector due to its versatility and capability to reduce emissions. However, many obstacles have prevented it from having yet a significant impact on energy systems at the present moment, such as costs and availability of specific infrastructure.

1.3 Literature Review

Section 1.3 contains the "Literature Review" and it is subdivided in four topics of research. Subsection 1.3.1 is a review about investigations of power losses in pipelines. Subsection 1.3.2 reviews works about numerical modelling and simulation of a gas transmission network. Afterwards, studies concerning the effects of injecting $\mathrm{H_2}$ in NG pipelines are examined in Subsection 1.3.3. The final topic to be approached is the economic analysis of $\mathrm{H_2}$ production projects in Subsection 1.3.4.

1.3.1 Power Losses in Pipelines

The first topic to be reviewed regards power losses in pipelines. First of all, power losses in pipeline transmission include both viscous frictional losses and losses due to heat transfer along the pipe. The viscous friction that is established between the fluid particles and the pipe walls is responsible for some energy dissipation when fluid travels in a pipe. This loss due to friction causes a pressure drop along the length of the pipe, therefore increasing the amount of power that a pump must deliver to maintain the flow, and they are significant in systems where long stretches of piping are employed (for example, pipelines). Fundamentally, a greater or lesser pressure loss in a pipe depends on various parameters, such as cross-section, length, flow rate, material, roughness, and the fluid itself. Also, minor appurtenances and accessories present in a pipe network can cause a sudden loss due to the change in magnitude, direction, or distribution of the velocity of the flow. However, those are neglectable in considerable long pipelines. On the other hand, there are mainly two mechanisms of heat transfer in pipelines. The first is conduction, which occurs when there is a thermal path between areas with different temperatures. A buried pipe, for example, has intimate contact with the backfill, setting up a thermal path from the gas through the pipe wall and insulation, into the soil or water surrounding it. The other heat transfer mechanism is convection, which results from fluid motion over a thermally active surface. Common examples include wind on an exposed or elevated pipeline, ocean currents over the submerged pipe, or the flow in the pipe passing over the internal surface of the pipe containing it. Depending on the specific situation, some heat transfer mechanisms may be more significant than others.

Power losses in both gas and electric systems were investigated by Jurado and Cano [27]. Through an IEEE 30-bus test system using MATLAB, Jurado and Cano concluded that, for shorter lengths, losses associated with the gas system are lower than for electric systems. Alternatively, the losses are larger for gas systems for longer distances, meaning that these power losses are relevant and should be thoroughly considered. In fact, energy losses in pipes used for the transmission of fluids have been immensely studied. Lahiounel and Haddad [28] conducted a study comparing different relationships to determine energy losses in a range of pipes of varying sizes and roughness used for the transmission of fluids with experimental results. The acquired linear results were compared to those obtained using the most used pipe flow formulas (Darcy-Weisbach, Hazen-Williams, Manning, Strickler, Scobey, and Calmon and Lechapt) to determine the domain of applicability and accuracy of these relationships. The experimental data, when compared to those computed using the relationships, demonstrated a preponderance of both the Darcy-Weisbach and Hazen-Williams correlations. The errors discovered

appear to be mostly related to the difficulty in calculating the friction coefficient, which is a function of the Reynolds number and roughness of the wall pipe. The challenging issue in determining pipe roughness is that such pipes are susceptible to the age effect, which leads to erosion, corrosion, and deposits. This invalidates the manufacturer's coefficient value.

Studies about power losses in NG transmission systems have also been contemplated. Particularly, Xie *et al.* [9] developed an energy efficiency model for a NG pipeline through the usage of an analytic hierarchy process. This model was established given that a long-distance NG pipeline is constituted of various pipe segments and components, which increases the difficulty of assessing the overall energy efficiency. Xie *et al.* established an energy efficiency index system, which comprised the energy efficiency coefficient at the compressor station, loss ratio, and energy efficiency coefficient of the pipeline.

As previously mentioned, the frictional drag loss is one of the parameters responsible for the power losses in a pipeline. Therefore, several studies have been effectuated within the scope of attempting to estimate the friction factor with accuracy. Sletfjerding and Gudmundsson [29] elaborated a new friction factor correlation in terms of direct measurement of roughness. The motivation for this work was based on the significant effects of the wall roughness on friction factors and velocity profiles in industrial applications with high Reynolds numbers. Therefore, this study presented experimental results of several pipes with varying wall roughness with high Reynolds numbers. When the wall roughness was high, the results of flow experiments, at high Reynolds numbers in pipes with roughened walls, demonstrated that the friction factor was independent of Reynolds number. It was discovered that measured friction factors correlated well with the root-mean-square roughness and slope of the power spectrum of the measured roughness profile. Between the friction factor that applies to rough flow and the directly observed wall roughness, a new correlation has been presented. The findings revealed that turbulent flow at high Reynolds numbers is highly sensitive to small changes in surface roughness.

Given the relevance of the frictional loss parameter, some experimental works have been conducted with the aim of reducing its negative effect. Huang *et al.* [30] addressed the problem related to the loss of energy due to frictional resistances in NG transmission by analysing the effect of using Drag Reduction Agent (DRA) technology on the pipe inner-surface roughness. Furthermore, the article by Ma *et al.* [31] synthesised a new DRA named Organic Carboxylate Polymer (CPA) and conducted an experimental investigation on the roughness-reducing effect on the inner surface of a NG pipe.

1.3.2 Numerical Modelling and Simulation of a Gas Transmission Network

There are several studies about the modelling and simulation of a gas transmission network, which is similar to the aim of the work developed in the present Dissertation.

The research of Herrán-González *et al.* [32] is about the model and simulation of a gas distribution network, with a specific emphasis on gas ducts. The main goal of this study was the implementation of a gas distribution pipeline network simulator using MATLAB-Simulink. Woldeyohannes and Majid [33] developed a simulation model for the NG transmission network system although focusing on compression stations, which was able to help decisions with regard to the design and operation of the transmission

network.

Concerning transient flow, Osiadacz and Gburzynska [34] compared mathematical models to describe transient flow inside a gas pipeline. Osiadacz and Gburzynska concluded that parabolic models are more simple to be numerically solved compared to hyperbolic models, and can be used for designing simulation programs, however, they describe changes occurring in the network with less accuracy. Also, Hafsi *et al.* [35] focused on studying a model approach of transient gas flows through the linearisation method. This linearisation model was employed in a typical gas network, and it verified the capability of this model to detect leaks in the network. Lastly, Behbahani-Nejad and Bagheri [36] developed a transient flow simulation for gas pipelines and networks based on the transfer function models and MATLAB-Simulink, which showed acceptable accuracy and use of computational resources.

As it can be verified, modelling gas transmission networks in computational tools is a topic being recently developed and of immense importance to simulate the fluid flow in this type of system. Through the development of this type of computational tool, more investigations can be effectuated to implement improvements in gas transmission networks. It is important to mention that the case of modelling a country's high-pressure gas network, which is the topic being studied in this work, has not been investigated as far as the Author is aware.

1.3.3 Effect of Injecting Hydrogen in NG Pipeline Transmission

Given the potential of $\mathrm{H_2}$ to start to decarbonise the NG network, it is of extreme relevance to deeply understand the influence of injecting $\mathrm{H_2}$ in the NG pipelines. This slow transitory stage is expected to take years if not decades, since an overnight transition to a fully operational $\mathrm{H_2}$ network is not possible. Therefore, this subject has been tremendously investigated in the last few years.

When $\mathrm{H_2}$ is added to NG, several changes occur in the thermo-physical properties that are significant for gas transmission. Schouten *et al.* [37] studied the influence of injecting $\mathrm{H_2}$ on thermodynamic properties and concluded that the energy density decreased when $\mathrm{H_2}$ is added. Also, the study performed by Schouten *et al.* analysed the $\mathrm{H_2}$ effect on the pressure drop in pipelines. Actually, it was established that the pressure gradient in the pipelines is larger when NG is transported compared to the mixture containing $\mathrm{H_2}$ if the same quantity of gas is transported on a volumetric basis. However, the opposite was verified if the same amount of gas is transported on the same energy basis instead of volumetric.

Deymi-Dashtebayaz *et al.* [38] also investigated the effect of $\mathrm{H_2}$ injection on NG thermo-physical properties. The $\mathrm{H_2}$ was verified to increase the upper and lower flammability limits, Lower Heating Value (LHV), Higher Heating Value (HHV), and compressibility factor. However, the Wobbe indices and density decreased when the $\mathrm{H_2}$ concentration increased. Abd *et al.* [39] also concluded that the presence of $\mathrm{H_2}$ in NG mixture reduces its density. Moreover, the work of Abd *et al.* also found that up to 2% of $\mathrm{H_2}$ concentration increases the viscosity of the typical NG whereas the opposite occurs for concentrations above 2%.

Pipelines are the most cost-effective, energy-efficient, and safest way to transport $\mathrm{H_2}$ over long distances [40]. The current lack of $\mathrm{H_2}$ infrastructure is one of the most significant barriers to the widespread

use of H_2. However, a possibility is to effectuate modifications to existing infrastructures to implement this new technology. There are proposals to inject H_2 into the existing NG grid, allowing for a faster and more cost-effective transition to H_2 energy transport.

Witkowski *et al.* [41] suggested the usage of existent NG infrastructure to transport H_2, to avoid the costs associated with the construction of a brand-new infrastructure exclusively dedicated to H_2 transmission. Quarton and Samsatli [42] also mentioned that partial H_2 injection could be an important step, however, to attain large-scale decarbonisation of gas grids, it would imply a complete conversion to H_2. On a more practical approach, Gondal and Sahin [43] examined the prospects of NG pipeline infrastructure in H_2 transmission and they concluded that a mixture up to 17% of H_2 concentration did not have any considerable effect while a concentration with over 17% of H_2 required modifications in the high-pressure pipeline as well as in end-user applications. Gondal [44] also stated that each element in a NG infrastructure has its own capability of accepting different H_2 concentrations. This research concluded that the compressors are the most H_2 limiting component in a transmission network, accepting only 10% of concentration. In the components of the distribution network and storage, a maximum of 50% of H_2 concentration is accepted, while in end-use appliances, a range of $20 - 50\%$ is tolerated. Furthermore, the work by Ogden *et al.* [45] concluded that transporting NG blended with H_2 appeared technically possible only with fractions between $5 - 15\%$ concentrations, although it could be expensive and need extensive assessment of each specific case. Altfeld and Pinchbeck [46] stated that only 10% can be tolerated depending on the situation. Finally, Messaoudani *et al.* [47] provided a brief summary of the hazards and safety of transporting H_2 in the NG grid, which denoted gaps of knowledge due to little experimental data.

Therefore, it can be understood the dubiety of the overall percentage of hydrogen acceptable in the NG network since each component has its own limitations. Hence, this topic lacks the establishment of reasonable percentages of hydrogen when transporting NG blended with hydrogen in the high-pressure network.

1.3.4 Economic Analysis of Hydrogen Production Projects

Since the investigations in Subsection 1.3.3 concerned the effects of injecting H_2 in a NG pipeline, it is also crucial to analyse the economic viability of producing such H_2 through electrolysis.

First of all, Schmidt *et al.* [48] analysed the future cost and performance of water electrolysis and concluded that by increasing the research and development funding, the capital cost is able to reduce by 0–24%. Also, the work of Schmidt *et al.* established that efficiency updates are negligible, and the lifetime of the system may converge at around $60000 - 90000$ hours.

In terms of innovations in the common electrolysers, Koj *et al.* [49] presented a new hybrid AEL with a Gas Diffusion Electrode (GDE) operating as the anode. This concept revealed to have the same cell potential when compared to an ordinary electrolysis cell and presented good electrochemical stability. Kumar and Humabindu [25] studied the PEMEL and considered it the most promising method to produce high pure efficient H_2 from renewable sources. The work of Xu and Scott [50] regarded the effects of

having Nafion ionomer context in membrane electrode assemblies of a polymer electrolyte PEMEL. Electrochemical studies showed that the optimal Nafion ionomer contents for anode and cathode were 25% and 20%, respectively. Brisse *et al.* [51] researched the influence of the operating temperature, humidity, and current density on the SOEL performance and remarkably high conversion efficiency was obtained. Also, the investigation of Brisse *et al.* concluded that the steam diffusion in the H_2/steam electrode is a relevant limitation.

Techno-economic evaluations were also performed regarding projects that produce H_2 on a large scale. Particularly, Nguyen *et al.* [52] performed a techno-economic analysis in a large-scale H_2 production plant. The option of electrolytic H_2 generation combined with underground storage was determined to be the cheapest, resulting in a Levelised Cost of Hydrogen (LCOH) of $3 - 3.3$ €/kg for AEL and $2.72 - 3.62$ €/kg for PEMEL electrolysis. The cost of electrolytic H_2 was $6 - 27\%$ more than the cost of steam CH_4 reforming at $2.56 - 2.87$ €/kg (without carbon capture). When carbon capture and storage were included, the cost became comparable to steam CH_4 reforming. Nguyen *et al.* also concluded that maximizing the usage of electrolytic systems through high capacity factors can be advantageous. The research of Matute *et al.* [53] proposed an advanced techno-economic model for calculating the optimal dispatch of multi-MW electrolysis plants on a large scale. This model was applied to Spain to determine the minimum demand from the fuel cell vehicle (FCEV) market. It was concluded that grid services contribute to the viability of H_2 production for mobility, even with a small but significant demand from FCEV fleets. Furthermore, Correa *et al.* [54] investigated the techno-economic viability of producing green H_2 in Argentine Patagonia to then be transported to Italy by ship. This economic assessment included the complete supply chain from its production using renewable energy sources to its usage as a fuel for mobility. The LCOH of the H_2 production, storage, and transportation was 8.6 €/kg. Fan *et al.* [55] compared the LCOH of H_2 production from coal-to-hydrogen process (C2H), low-carbon H_2 production technologies such as C2H coupled with carbon capture and storage (C2HCCS) and renewable water electrolysis. Fan *et al.* stated that the LCOH of C2HCCS is $1.86 - 2.75$ €/kg, which is $57.6 - 128.3\%$ higher than C2H. Also, it is $20.6 - 61.0\%$ lower than H_2 water electrolysis, whose LCOH is $2.32 - 7.34$ €/kg. The work of Minutillo *et al.* [56] focused on a techno-economic assessment in refuelling stations with H_2 electrolysis. The findings revealed that investment costs rise proportionally as the electricity mix shifts from full grid operation to low grid supply and as H_2 production capacity increases. Considering the yearly cost of power acquired from the grid, operating and maintenance expenditures are the largest contribution to the LCOH. The project's LCOH ranged from $9.29 - 12.48$ €/kg.

Therefore, it can be verified that some of these types of projects are economically feasible, however, it depends on the characteristics of each project.

1.4 Objectives

The main objective of the present Dissertation is to analyse the power losses associated with the transmission of natural gas and hydrogen in the Portuguese high-pressure network. Particularly, this work aims to:

- Create and validate the computational tool which computes the required mass flow rate to answer the energy demand of the Portuguese major industrial consumers as well as the power losses associated to its transmission;
- Establish the influence of each parameter, such as mass flow rate, hydraulic diameter, length, and roughness, on the power losses for a simplified model;
- Define scenarios within the RNTGN to comprise several supply options and compute the power losses associated to the NG transmission to supply the Portuguese major industrial consumers for the defined scenarios;
- Analyse the influence of blending several percentages of $\mathrm{H_2}$ in the NG mixture on the power losses for the same scenarios;
- Study the economic viability of producing the $\mathrm{H_2}$ to be blended in the NG mixture; and
- Assess the economic impact on the industries of using the blended mixture with those several percentages of $\mathrm{H_2}$ and the associated $\mathrm{CO_2}$ emissions reduction.

Essentially, this work aspires to assist the beginning of the decarbonisation path in the Portuguese network. Even though this work does not present the complete solution to cease the dependence on natural gas, it contemplates mixtures with small percentages of hydrogen to start to understand further implications of future usage of the Portuguese network to transport exclusively hydrogen, such as the power losses associated with its transmission.

1.5 Dissertation Outline

The structure of the Dissertation begins with Chapter 1, which includes the ”Motivation”, ”Description and Overview”, ”Literature Review”, ”Objectives” and the present ”Dissertation Outline”. Chapter 2 comprises the ”Theoretical Background” regarding both the numerical and economic model. Chapter 3 is the ”Implementation”, once again, of the developed numerical model and economic assessment model. Chapter 4 regards the ”Results and Discussion”, including the ”Model Validation”, ”Parametric Study”, and ”Case of Study”, which contemplates the ”Power Losses Study”, ”Influence of Blending $\mathrm{H_2}$ Study”, ”Economic Assessment of $\mathrm{H_2}$ Production”, and ”Economic Impact Study on the Industry”. Finally, Chapter 5 are the ”Conclusions” where the ”Achievements” and ”Future Work” are described.

Chapter 2

Theoretical Background

Chapter 2 presents the governing equations incorporated in both the numerical and economic assessment models. Particularly, the Section 2.1 regards the numerical model and Section 2.2 presents the economic equations utilised in the economic assessment model.

2.1 Numerical Model

In Section 2.1, the theoretical background behind the numerical model is described. Firstly, the governing equations are presented in Subsection 2.1.1, adapted from [57]. Then, the assumptions and limitations of the developed numerical model are stated in Subsection 2.1.2.

2.1.1 Model Equations

Firstly, the mass balance inside a control volume can be written as in Equation (2.1), which relates the dynamics of pressure and temperature of the internal node representing the gas volume to the inlet and outlet mass flow rates. Concretely, it describes the mass conservation of the flow inside a pipeline within a gas network, where $\frac{\partial M}{\partial p}$ is the partial derivative of the gas volume mass concerning pressure at constant temperature and volume, $\frac{\partial M}{\partial T}$ is the partial derivative of the gas volume mass respecting temperature at constant pressure and volume, p_{I} [MPa] is the pressure of the gas volume, T_{I} [K] is the temperature of the gas volume, t is time, $\dot{m}_{\mathrm{in}}$ [$\mathrm{kg/s}$] and $\dot{m}_{\mathrm{out}}$ [$\mathrm{kg/s}$] are mass flow rates at inlet and outlet, respectively.

$$\frac{\partial M}{\partial p} \cdot \frac{dp_{\mathrm{I}}}{dt} + \frac{\partial M}{\partial T} \cdot \frac{dT_{\mathrm{I}}}{dt} = \dot{m}_{\mathrm{in}} + \dot{m}_{\mathrm{out}} \tag{2.1}$$

Secondly, the energy balance is presented in Equation (2.2), which is essentially the first law of thermodynamics for a control volume. This conservation equation establishes a corresponding between the dynamics of pressure and temperature of the internal representing the gas volume and the energy and heat flow rates. The term $\frac{\partial U}{\partial p}$ is the partial derivative of internal energy of the gas volume with regard to the pressure at constant temperature and volume, $\frac{\partial U}{\partial T}$ is the partial derivative of internal energy of the

gas volume with regard to the temperature at constant pressure and volume, Φ_{in} [W] and Φ_{out} [W] are energy flows at the inlet and outlet, respectively, and q_{sur} [W] is the heat flow rate from the surroundings.

$$\frac{\partial U}{\partial p} \cdot \frac{dp_{\mathrm{I}}}{dt} + \frac{\partial U}{\partial T} \cdot \frac{dT_{\mathrm{I}}}{dt} = \Phi_{\mathrm{in}} + \Phi_{\mathrm{out}} + q_{\mathrm{sur}} \tag{2.2}$$

The momentum balances written in Equations (2.3a) and (2.3b) are also known as the Bernoulli's Equation, though not considering the gravitational potential energy term since the pipeline is assumed to be all at the same height. The pressure drop caused by momentum flux and viscous friction is described by the conservation of momentum for each half of the pipe, as presented in Equations (2.3a) and (2.3b) for the first and second half, respectively. The terms p and ρ [$\mathrm{kg/m^3}$] are the pressure and density at inlet, outlet, or internal node, as indicated by each subscript, and the term S [$\mathrm{m^2}$] is the pipe cross-sectional area. The terms $\Delta p_{\mathrm{in,I}}$ and $\Delta p_{\mathrm{out,I}}$ are the pressure losses due to viscous friction.

$$p_{\mathrm{in}} - p_{\mathrm{I}} = \left(\frac{\dot{m}_{\mathrm{in}}}{S}\right)^2 \cdot \left(\frac{1}{\rho_{\mathrm{I}}} - \frac{1}{\rho_{\mathrm{in}}}\right) + \Delta p_{\mathrm{in,I}} \tag{2.3a}$$

$$p_{\mathrm{out}} - p_{\mathrm{I}} = \left(\frac{\dot{m}_{\mathrm{out}}}{S}\right)^2 \cdot \left(\frac{1}{\rho_{\mathrm{I}}} - \frac{1}{\rho_{\mathrm{out}}}\right) + \Delta p_{\mathrm{out,I}} \tag{2.3b}$$

The momentum balances for both halves of the pipe presented in Equations (2.3a) and (2.3b) are assumed to be adiabatic processes since the heat exchanged with the pipe wall is already summed to the energy of gas me in Equation (2.2). Hence, the adiabatic relations related to both momentum balances are written in Equations (2.4a) and (2.4b) for the first and second half of the pipe, respectively. The term h [$\mathrm{J/kg}$] represents the specific enthalpy at the inlet, outlet, or internal node, depending on the subscript.

$$h_{\mathrm{in}} + \frac{1}{2}\left(\frac{\dot{m}_{\mathrm{in}}}{\rho_{\mathrm{in}} S}\right)^2 = h_{\mathrm{I}} + \frac{1}{2}\left(\frac{\dot{m}_{\mathrm{in}}}{\rho_{\mathrm{I}} S}\right)^2 \tag{2.4a}$$

$$h_{\mathrm{out}} + \frac{1}{2}\left(\frac{\dot{m}_{\mathrm{out}}}{\rho_{\mathrm{out}} S}\right)^2 = h_{\mathrm{I}} + \frac{1}{2}\left(\frac{\dot{m}_{\mathrm{out}}}{\rho_{\mathrm{I}} S}\right)^2 \tag{2.4b}$$

Followingly, the calculation of the pressure losses due to viscous friction depends on the flow regime. Thus, the Reynolds number on both halves of the pipe must be computed through Equations (2.5a) and (2.5b), where D_{hyd} [m] is the hydraulic diameter of the pipe and μ_{I} [$\mathrm{Pa \cdot s}$] is the dynamic viscosity at internal node.

$$\mathrm{Re}_{\mathrm{in}} = \frac{|\dot{m}_{\mathrm{in}}| \cdot D_{\mathrm{hyd}}}{S \cdot \mu_{\mathrm{I}}} \tag{2.5a}$$

$$\mathrm{Re}_{\mathrm{out}} = \frac{|\dot{m}_{\mathrm{out}}| \cdot D_{\mathrm{hyd}}}{S \cdot \mu_{\mathrm{I}}} \tag{2.5b}$$

For the flow circulating inside the pipe on a turbulent flow regime, the pressure losses caused by viscous friction are determined using Equations (2.6a) and (2.6b). The term f_{Darcy} is the Darcy friction

factor at the inlet or outlet, as indicated by the subscript, and term L [m] is the pipeline's length.

$$\Delta p_{\mathrm{in,I_{turb}}} = f_{\mathrm{Darcy_{in}}} \frac{\dot{m}_{\mathrm{in}} \cdot |\dot{m}_{\mathrm{in}}|}{2\rho_{\mathrm{I}} \cdot D_{\mathrm{hyd}} \cdot S^2} \cdot \frac{L + L_{\mathrm{eqv}}}{2} \tag{2.6a}$$

$$\Delta p_{\mathrm{out,I_{turb}}} = f_{\mathrm{Darcy_{out}}} \frac{\dot{m}_{\mathrm{out}} \cdot |\dot{m}_{\mathrm{out}}|}{2\rho_{\mathrm{I}} \cdot D_{\mathrm{hyd}} \cdot S^2} \cdot \frac{L + L_{\mathrm{eqv}}}{2} \tag{2.6b}$$

Particularly, the Darcy friction factors are calculated through the Haaland correlation, as presented in Equations (2.7a) and (2.7b), where ε [m] is the internal surface absolute roughness parameter value.

$$f_{\mathrm{Darcy_{in}}} = \left[-1.8 \log \left(\frac{6.9}{\mathrm{Re_{in}}} + \left(\frac{\varepsilon}{3.7 D_{\mathrm{hyd}}} \right)^{1.11} \right) \right]^{-2} \tag{2.7a}$$

$$f_{\mathrm{Darcy_{out}}} = \left[-1.8 \log \left(\frac{6.9}{\mathrm{Re_{out}}} + \left(\frac{\varepsilon}{3.7 D_{\mathrm{hyd}}} \right)^{1.11} \right) \right]^{-2} \tag{2.7b}$$

On the other hand, the convective heat transfer equation between the internal gas volume and the pipe wall is presented in Equation (2.8).

$$q_{\mathrm{sur}} = q_{\mathrm{cond}} + q_{\mathrm{conv}} \tag{2.8}$$

The conductive heat transfer is calculated with Equation (2.9), where $S_{\mathrm{surf}} = \frac{4SL}{D_{\mathrm{hyd}}}$ is the pipe surface area and k [$\mathrm{W/m \cdot K}$] is the thermal conductivity. Equation (2.9) can also be adapted to compute the conduction between multiple layers, in case of the presence of insulation.

$$q_{\mathrm{cond}} = \frac{k_{\mathrm{I}} S_{\mathrm{surf}}}{D_{\mathrm{hyd}}} \left(T_{\mathrm{sur}} - T_{\mathrm{I}} \right) \tag{2.9}$$

The convective heat transfer term can be computed through Equation (2.10), considering an exponential temperature distribution along the pipe. The term $\dot{m}_{\mathrm{avg}}$ is the average mass flow rate between the pipe's inlet and outlet, and the term $c_{\mathrm{p_{avg}}}$ [$\mathrm{J/kg \cdot K}$] is the specific heat evaluated at the average temperature.

$$q_{\mathrm{conv}} = |\dot{m}_{\mathrm{avg}}| \, c_{\mathrm{p_{avg}}} \left(T_{\mathrm{sur}} - T_{\mathrm{in}} \right) \left(1 - \exp \left(- \frac{h S_{\mathrm{surf}}}{|\dot{m}_{\mathrm{avg}}| \, c_{\mathrm{p_{avg}}}} \right) \right) \tag{2.10}$$

Besides, the heat transfer coefficient h [$\mathrm{W/m^2 \cdot K}$] is determined using Equation (2.11), where k_{avg} is the thermal conductivity at the average temperature.

$$h = Nu \frac{k_{\mathrm{avg}}}{D_{\mathrm{hyd}}} \tag{2.11}$$

More concretely, the Nusselt number is dependent on the flow regime. Since the flow is on the turbulent flow regime, the Nusselt number is computed through the Gnielinski correlation presented in Equation (2.12). The term Pr_{avg} [$\mathrm{m^2/s}$] is the Prandtl number at the average temperature.

$$Nu_{\mathrm{turb}} = \frac{\frac{f_{\mathrm{Darcy}}}{8} \left(\mathrm{Re_{avg}} - 1000 \right) \mathrm{Pr_{avg}}}{1 + 12.7 \sqrt{\frac{f_{\mathrm{Darcy}}}{8}} \left(\mathrm{Pr_{avg}^{2/3}} - 1 \right)} \tag{2.12}$$

Finally, the average Reynolds number is calculated through Equation (2.13), where μ_{avg} is the dynamic viscosity evaluated at average temperature.

$$\mathrm{Re}_{\mathrm{avg}} = \frac{|\dot{m}_{\mathrm{avg}}|\, D_{\mathrm{hyd}}}{S\mu_{\mathrm{avg}}} \tag{2.13}$$

2.1.2 Assumptions and Limitations

The developed numerical model considers the following:

- The governing equations are solved for steady-state;
- The pipe wall is perfectly rigid;
- The flow is fully developed, meaning that friction losses and heat transfer do not include any entry influence;
- The effect of gravity is negligible; and
- The fluid inertia is also negligible.

2.2 Economic Assessment Model Equations

The LCOH calculation is performed through Equation (2.14). This computation must be determined to estimate the approximate cost of H_2 production and to establish its competitiveness in the market. The term I_{t} is related to the capital expenditures (CAPEX) in year t, O_{t} considers the operation expenditures (OPEX) in year t, F_{t} accounts for the electricity costs, and E_t is the total quantity of H_2 produced in year t. The rate of return on investment is denoted by r and the lifetime of the project is represented by n.

$$LCOH = \frac{\sum_{t=1}^{n} \frac{I_{\mathrm{t}}+O_{\mathrm{t}}+F_{\mathrm{t}}}{(1+r)^{\mathrm{t}}}}{\sum_{t=1}^{n} \frac{E_{\mathrm{t}}}{(1+r)^{\mathrm{t}}}} \tag{2.14}$$

The Net Present Value (NPV) is the difference between discounted cash inflows (revenues) and outflows (expenses) during the project lifetime. It is computed using Equation (2.15), where CF_t stands for the cash-flow in year t and I_0 is the investment.

$$NPV = \sum_{t=1}^{n} \frac{CF_{\mathrm{t}}}{(1+r)^{\mathrm{t}}} - I_0 \tag{2.15}$$

This economic assessment index is used to determine the economic viability of the project. If the NPV is positive indicates viability, meaning that the results achieved cover the expenses and generate a financial surplus. However, if the NPV is negative, the project is economically non-viable.

The Internal Rate of Return (IRR) is the discount rate at which the NPV equals zero, which translates in being the minimum rentability that an investor lending institution aims to obtain from the project. The IRR is calculated through Equation (2.16).

$$0 = \sum_{t=1}^{n} \frac{CF_{\mathrm{t}}}{(1+IRR)^{\mathrm{t}}} - I_0 \tag{2.16}$$

If the obtained IRR is greater than the r previously considered in the project, it indicates the ability of the project to generate a rate of return higher than the opportunity cost of capital. However, if the IRR is lesser than r, it means that the required minimum profitability is not attained.

Finally, the Payback Period (PBP) is the number of years necessary to recover the cost of an investment. This value is determined using Equation (2.17).

$$PBP = \sum_{t=1}^{n} \frac{I_0}{CF_{\mathrm{t}}} \tag{2.17}$$

Chapter 3

Implementation

Chapter 3 regards the implementation of the created computational tool. It includes the description of both the numerical and economic assessment models in Sections 3.1 and 3.2, respectively.

3.1 Numerical Model

The numerical model is developed with the aim of computing the power loss inside a pipeline transporting NG. This model developed in Simulink is the core of the computational tool created in MATLAB-Simulink that is further applied to a specific case of study. Thus, Subsection 3.1.1 explains the methodology for the development of the simplified model and case of study. Further, Subsection 3.1.2 defines the properties of the gases considered in the created computational tool.

3.1.1 Methodology

As previously referred, the created numerical model is the foundation of the developed computational tool. The methodology behind the conception of the simplified model is explained next. The simplified model is a more straightforward concept that is then developed to be applied to the complex case of study.

Simplified Model

The simplified model serves as the base of the created computational tool, and it consists of a basic configuration composed of Simscape blocks representing two reservoirs, at left (labelled as A) and at right (labelled as B), a mass flow rate source (labelled as C), and a single pipe (labelled as D), as represented in the schematic of Figure 3.1. Both left and right reservoirs are maintained at the same pressure and temperature. The mass flow rate source block represents an ideal mechanical energy source in the network, maintaining a constant mass flow rate flowing in the required direction. This block acts as a compressor in the system since the pressure increases when the gas flows through it. The pipe block is connected to other three blocks that account for the thermal contribution related to the

conduction between the soil, the insulation, and the pipe. Besides, there are several sensors distributed through this layout, which include both pressure and temperature sensors (labelled as E) as well as mass flow rate and power sensors (labelled as F). Through these sensors, it is possible to compute the pressure drop in the pipe through the difference in pressure between the sensor immediately after and before the pipe. It is also achievable the computation of the power losses associated with the transmission inside this pipe by dividing the power measured immediately after and before the pipe. Further on, this simplified model is validated in Section 4.1.

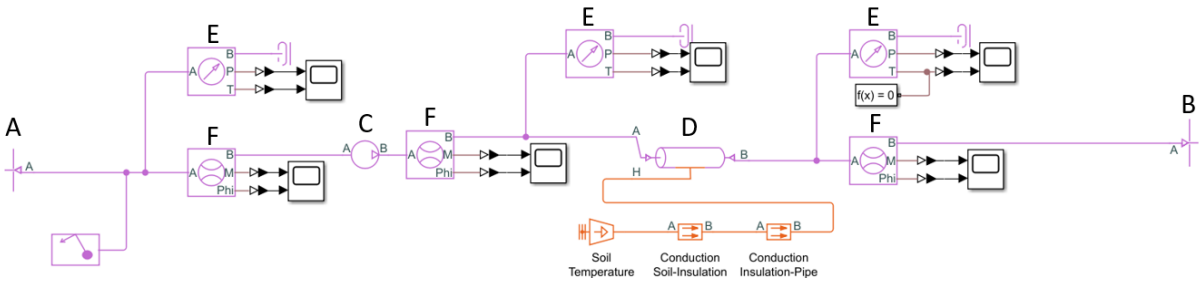

Figure 3.1: Simplified model in MATLAB-Simulink, in which the gas flows from left (A) to right (B).

Case of Study

As previously mentioned in Subsection 1.2.1, the Portuguese industry has a preponderant role in the national NG demand. For such, the case of study addresses the supply of those industries through the RNTGN, and the objective is for the computational tool to compute the required NG mass flow rate to satisfy the demand of the Portuguese major industrial consumers, as well as the power losses associated with its transmission. Beforehand, the list of the CO_2-emitting Portuguese industry taken into consideration in the model is presented in Appendix A.1, which is adapted from [58]. This list includes all the industries that have attributed licenses for emitting CO_2 in Portugal, and they can be either high-pressure or distribution network clients. These industries are listed in geographical order presenting the maximum allowed amount of CO_2 that each one emits gratuitously in a year. Also, Figure 3.2 shows the quantity of CO_2 licenses *per* industrial sector, from [58], in which can be verified the evident dominance of the Chemical and Petrochemical, and Mining and Extracting sectors.

However, first, it is essential to mention that the simplification of NG being constituted by 100% of CH_4 is assumed in this case of study. Considering the balanced CH_4 combustion reaction presented in Equation (3.1), the stoichiometry of Equation (3.2) can be stated. Hence, through the data regarding the licensed quantity of emitted CO_2 and assuming a constant supply during 24 hours in all 365 days, the required mass flow rate to satisfy the demand of each industry is computed.

$$CH_4 + 2O_2 \Longrightarrow CO_2 + 2H_2O \tag{3.1}$$

$$n_{CH_4} = n_{CO_2} \tag{3.2}$$

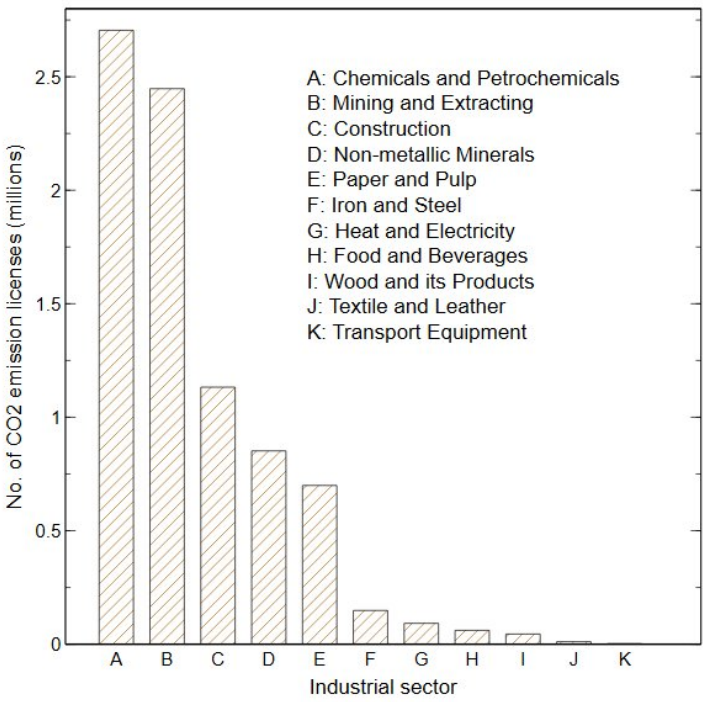

Figure 3.2: Number of $\mathrm{CO_2}$ emission licenses attributed *per* industrial sector.

Figure 3.3 illustrates the map of Portugal where the total NG mass flow rate required by each district is observable, computed through the procedure described above. One can conclude that the majority of the Portuguese industrial consumers is located in the littoral of Portugal, coinciding with the RNTGN placement.

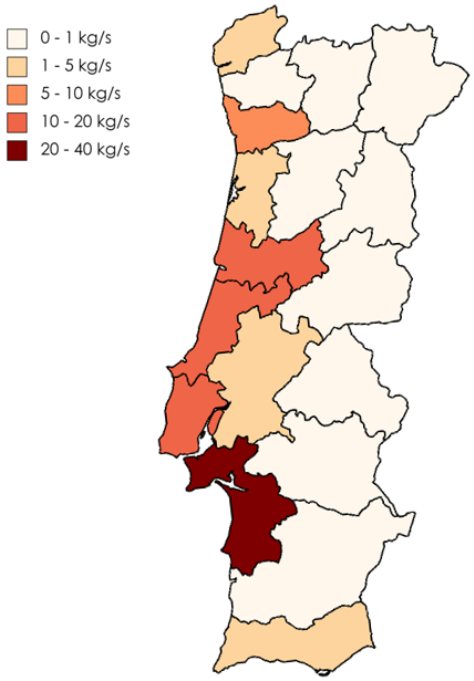

Figure 3.3: Required NG mass flow rate [$\mathrm{kg/s}$] for the industrial consumers in each Portuguese district.

In the computational tool, the RNTGN represented in Figure 3.4 is divided into several pipeline segments, as summarized in Table 3.1. The characteristics of each segment, namely the hydraulic diameter and length are based on [59]. The considered internal absolute roughness is $50 \cdot 10^{-6}$ m in all RNTGN since the pipeline segments were built over a year ago [60].

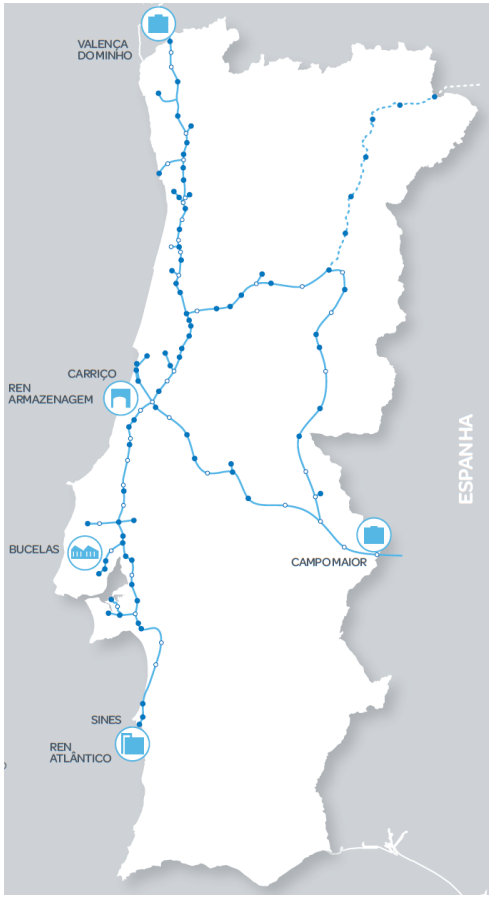

Figure 3.4: Portuguese Natural Gas Transmission Network, from [16].

Table 3.1: RNTGN pipeline segments considered in the computational tool, from [59].

Segment	Subsegment	D_{hyd} [m]	L [km]
Sines – Setúbal		0.8	87
Setúbal – Bidoeira		0.7	174
Bidoeira – Campo Maior		0.7	220
Bidoeira – Figueira da Foz		0.7	19
Bidoeira – Cantanhede		0.7	64
Cantanhede – Monforte	Cantanhede – Mangualde	0.5	68
	Mangualde – Celorico	0.7	48
	Celorico – Guarda	0.3	29
	Guarda – Monforte	0.3	184
Cantanhede – Valença do Minho	Cantanhede – Gondomar	0.7	100
	Gondomar – Braga	0.5	50
	Braga – Valença do Minho	0.7	100

Every industry, or group of nearby industries, is connected to the nearest segment of the high-pressure pipeline through ramifications, which transport the mass flow rate necessary to feed the respective demand. Each segment has a similar configuration as the simplified model, although considering ramifications to link it to each group of nearby industries. For example, Figure 3.5 is the configuration between Sines (labelled as G) and Setúbal (labelled as H) developed in Simulink, where two vertical ramifications can be observed. Particularly, the first ramification (labelled as I) connects the principal high-pressure pipeline to Refinaria Sines Petrogal, Repsol Polímeros, and Indorama Ventures, transporting the NG mass flow rate necessary to satisfy all three of them. These three industries are grouped together as a simplification, and this simplification is considered when the industries are geographically proximate. The second ramification (labelled as J) connects the main pipeline to Euroresinas, only delivering the supply demanded by this company.

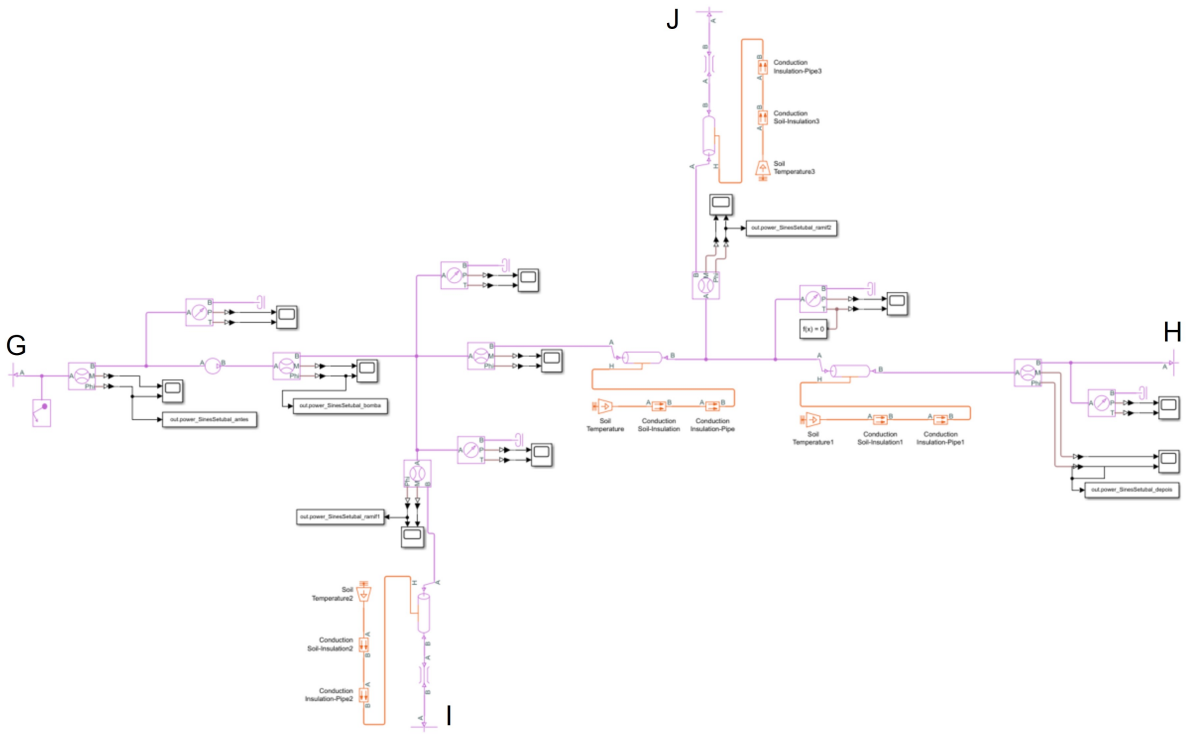

Figure 3.5: Segment Sines-Setúbal in MATLAB-Simulink, in which the gas flows from G to H, I, and J.

Finally, this model also accounts for the LNG Terminal at Sines, the two interconnections to Spain: Campo Maior and Valença do Minho, as well as the caverns of Carriço Underground Gas Storage. The connection to Carriço Underground Gas Storage is effectuated through a ramification from the segment Bidoeira-Figueira da Foz.

The computational tool considers the NG mass flow rate input in the LNG Terminal at Sines, which is represented in the left reservoir and mass flow rate source in the Simulink between Sines and Setúbal, as can be observed in Figure 3.5. Followingly, all the segments are interconnected in the correct geographical order through a MATLAB program. The mass flow rate input of the following segment is equal to the output of the previous segment, which means that the program always considers the remaining

mass flow rate from the principal pipeline since a certain amount exited through ramifications to the respective industries.

The main aim of this computational tool is to compute the power losses associated with gas transmission inside the RNTGN. The overall power loss is computed through an energy balance that considers as input the mass flow rate entering the segment Sines-Setúbal with the quantity required to feed the majority of the Portuguese industrial consumers, as well as the power provided by the mass flow rate source and the minor difference at the segments interconnection. Moreover, the output considers all the powers measured at the end of each ramification of the segments, as well as the residual remaining exiting mass flow rate at the end of the segment Cantanhede-Valença do Minho. For that, the computation of the overall power loss requires power measurements with sensors in each segment. More concretely, for each segment, the power needs to be measured before and after the mass flow rate source. Then, it is also measured at the end of each ramification as well as at the end of the main pipe.

The created computational tool models the case of study, which consists of the entire RNTGN supplying the Portuguese major industrial consumers with the NG mass flow rate necessary to feed its demand. The case of study includes different supply scenarios, for which the results are obtained for the transmission of NG in the RNTGN. The considered scenarios are the following:

(A) Industrial Supply Scenario: LNG Terminal at Sines supplying the Portuguese industrial consumers;

(B) Exportation Scenario: LNG Terminal at Sines supplying the Portuguese industrial consumers and exporting 10% to Spain;

(C) Storage Scenario: LNG Terminal at Sines supplying the Portuguese industrial consumers and filling the caverns of Carriço Underground Gas Storage; and

(D) Industrial Supply from Storage Scenario: Carriço Underground Gas Storage and LNG Terminal at Sines supplying the Portuguese industrial consumers.

Scenario (A) consists of LNG Terminal at Sines supplying NG to Portuguese industrial consumers. Followingly, Scenario (B) involves the supply of the same industries as well as the exportation of NG to Spain. The value to be exported is about 10% of the energy required to supply the Portuguese industrial consumers. This scenario comprises three possible alternatives of exportation, such as, through Valença do Minho (B.1), Campo Maior (B.2), and both simultaneously (B.3). Scenario (C) accounts for both the supply of the Portuguese industrial consumers and the fill of the caverns of Carriço Underground Gas Storage. However, due to constraints in the caverns' injection capability [16], only a certain amount of NG can be injected *per* second (C.1). It is also considered a hypothetical case where the injection capability of the caverns is doubled (C.2). The injection capability could be doubled in case of increasing the number of operating caverns, or even doubling the volume capacity of the caverns. Given that Scenario (C) injected NG to fill the caverns, now Scenario (D) consists of supplying the Portuguese industrial consumers through the usage of the NG stored in the caverns of Carriço Underground Gas Storage. Once again, there are constraints in the caverns' extraction capability [16], limiting the maximum quantity of NG that can be extracted *per* second. However, this quantity is not enough to satisfy

the total demand. Therefore, it is also required for the LNG Terminal at Sines to supply the remaining NG.

Since one of the objectives of the present Dissertation is to contribute to slowly starting to decarbonise the Portuguese network by studying the injection of higher percentages of $\mathrm{H_2}$ in the RNTGN, the developed computational tool is also applied for NG blended with several percentages of $\mathrm{H_2}$: $5\%_{\mathrm{vol}}$, $10\%_{\mathrm{vol}}$, and $20\%_{\mathrm{vol}}$ of $\mathrm{H_2}$. However, when introducing $\mathrm{H_2}$, the mass flow rate required to satisfy the Portuguese industrial consumers is different for the same energy, due to $\mathrm{H_2}$ different LHV, as verified with detail in the next subsection. Essentially, the aim is to compare the power losses in the transmission of NG and of NG blended with $\mathrm{H_2}$, to directly understand the impact of this blend.

3.1.2 Gas Properties

In the present Subsection, the thermo-physical properties of the gases utilised in the computational tool, namely $\mathrm{CH_4}$ and $\mathrm{H_2}$, are defined. The properties contemplated are density, molar mass, lower heating value, specific gas constant, compressibility factor, specific heat ratio, dynamic viscosity, and thermal conductivity. As explained in the previous Subsection, the case of study assumes that NG is constituted exclusively by $\mathrm{CH_4}$. The properties of these components are obtained for a p equal to $8\ \mathrm{MPa}$ and a T equal to $300\ \mathrm{K}$, and they are summarized in Table 3.2.

Table 3.2: Properties of the components at p equal to $8\ \mathrm{MPa}$ and a T equal to $300\ \mathrm{K}$.

Component	$\mathrm{CH_4}$	$\mathrm{H_2}$
ρ [$\mathrm{kg/m^3}$]	51.32	6.41
M [$\mathrm{kg/kmol}$]	16.04	2.02
LHV [$\mathrm{kWh/kg}$]	13.90	33.30
R [$\mathrm{kJ/kgK}$]	0.52	4.16
Z	0.88	1.05
C_{p} [$\mathrm{kJ/kgK}$]	2.23	14.43
$\mu \cdot 10^{-6}$ [$\mathrm{Pa.s}$]	13.10	8.89
k [$\mathrm{mW/mK}$]	34.10	186.90

Subsequently, the properties of the mixture composed of $\mathrm{CH_4}$ and $\mathrm{H_2}$ are estimated. Once again, the considered percentages of $\mathrm{H_2}$ are $5\%_{\mathrm{vol}}$, $10\%_{\mathrm{vol}}$, and $20\%_{\mathrm{vol}}$. First of all, the density of the mixture is computed through a weighted-average between both components considering the volume percentages, as presented in Equation (3.3).

$$\rho_{\mathrm{mix}} = \%_{\mathrm{vol}}[\mathrm{H_2}] \cdot \rho_{\mathrm{H_2}} + \%_{\mathrm{vol}}[\mathrm{CH_4}] \cdot \rho_{\mathrm{CH_4}} \tag{3.3}$$

For computing the LHV of the mixture, a weighted-average is also effectuated but considering the mass fraction of each component, as represented in Equation (3.4).

$$\mathrm{LHV}_{\mathrm{mix}} = \%_{\mathrm{mass}}[\mathrm{H_2}] \cdot \mathrm{LHV}_{\mathrm{H_2}} + \%_{\mathrm{mass}}[\mathrm{CH_4}] \cdot \mathrm{LHV}_{\mathrm{CH_4}} \tag{3.4}$$

The specific gas constant of the mixture can be also determined through a weighted-average between both component taking into consideration both mass fractions, as in Equation (3.5).

$$R_{\mathrm{mix}} = \%_{\mathrm{mass}}[\mathrm{H_2}] \cdot R_{\mathrm{H_2}} + \%_{\mathrm{mass}}[\mathrm{CH_4}] \cdot R_{\mathrm{CH_4}} \tag{3.5}$$

On the other hand, the calculation of the compressibility factor is done using Equation (3.6), which is weighted-average considering the volume percentages of each component of the mixture.

$$Z_{\mathrm{mix}} = \%_{\mathrm{vol}}[\mathrm{H_2}] \cdot Z_{\mathrm{H_2}} + \%_{\mathrm{vol}}[\mathrm{CH_4}] \cdot Z_{\mathrm{CH_4}} \tag{3.6}$$

The specific heat ratio is determined by a weighted-averaged that considers the mass fractions of each component, and it is presented in Equation (3.7).

$$C_{\mathrm{p_{mix}}} = \%_{\mathrm{mass}}[\mathrm{H_2}] \cdot C_{\mathrm{p_{H_2}}} + \%_{\mathrm{mass}}[\mathrm{CH_4}] \cdot C_{\mathrm{p_{CH_4}}} \tag{3.7}$$

Followingly, the dynamic viscosity is calculated similarly as the specific heat ratio, as seen in Equation (3.8).

$$\mu_{\mathrm{mix}} = \%_{\mathrm{mass}}[\mathrm{H_2}] \cdot \mu_{\mathrm{H_2}} + \%_{\mathrm{mass}}[\mathrm{CH_4}] \cdot \mu_{\mathrm{CH_4}} \tag{3.8}$$

Finally, the thermal conductivity can be determined through Equation (3.9).

$$k_{\mathrm{mix}} = \%_{\mathrm{mass}}[\mathrm{H_2}] \cdot k_{\mathrm{H_2}} + \%_{\mathrm{mass}}[\mathrm{CH_4}] \cdot k_{\mathrm{CH_4}} \tag{3.9}$$

Therefore, all the properties can be computed through all the equations presented for the three percentages of blended $\mathrm{H_2}$: $5\%_{\mathrm{vol}}$, $10\%_{\mathrm{vol}}$, and $20\%_{\mathrm{vol}}$. Table 3.3 shows all these computed properties.

Table 3.3: Properties for the mixtures with several percentages of $\mathrm{H_2}$ at p equal to $8\ \mathrm{MPa}$ and a T equal to $300\ \mathrm{K}$.

Mixture	95% $\mathrm{CH_4}$ + 5% $\mathrm{H_2}$	90% $\mathrm{CH_4}$ + 10% $\mathrm{H_2}$	80% $\mathrm{CH_4}$ + 20% $\mathrm{H_2}$
ρ [$\mathrm{kg/m^3}$]	49.07	46.83	42.34
LHV [$\mathrm{kWh/kg}$]	14.03	14.16	14.48
R [$\mathrm{kJ/kg \cdot K}$]	0.54	0.57	0.63
Z	0.89	0.90	0.91
C_{p} [$\mathrm{kJ/kg \cdot K}$]	2.31	2.39	2.59
$\mu \cdot 10^{-6}$ [$\mathrm{Pa \cdot s}$]	13.07	13.04	12.97
k [$\mathrm{mW/m \cdot K}$]	35.09	36.17	38.69

It can be verified that the presence of $\mathrm{H_2}$ decreases the density of the mixture and the dynamic viscosity, as in [38] and [39]. On the other hand, more $\mathrm{H_2}$ in the mixture translates into an increase of the LHV, specific gas constant, compressibility factor, heat capacity ratio, and thermal conductivity, as also in [38] and [39].

Hence, these mixture properties are the ones considered in the computational tool when the results are obtained for the case of the gas containing several percentages of $\mathrm{H_2}$.

3.2 Economic Assessment Model

After developing a numerical model integrated into a computational tool capable of computing the power losses associated with both the transmission of NG and NG blended with $\mathrm{H_2}$, the following step is to verify the economic viability of such a project.

With this aim, an economic assessment model is developed to study the economic viability of the production of $\mathrm{H_2}$ to blend with the NG that is transported to the industry. This analysis is focused on the perspective of a private $\mathrm{H_2}$ producer located adjacent to the LNG Terminal at Sines. Hence, it contemplates exclusively the production of $\mathrm{H_2}$, which means that this study does not regard the costs of the transmission and storage in the RNTGN since the same infrastructure is used. Regardless, the power losses related to its transmission computed through the developed computational tool are incorporated in this economic model in the sense that, by considering the production of the $\mathrm{H_2}$ quantity required to feed the Portuguese major industrial consumers, it is also produced the extra amount related to the power loss, so the industry receives the demanded energy.

This economic assessment includes the computation of some economic indicators such as LCOH, NPV, IRR, and PBP, using the equations described in Subsection 2.2. For the calculation of these indicators, several assumptions are made. Firstly, the rate of return on investment r for the project is assumed 8% [61] and this analysis takes no account of financial costs incurred as a result of credit interest or equity raising. Even though the corporate income tax rate in Portugal is around 31.5% [62], an income tax of 20% is considered in the present study assuming that exists political encouragement to develop this type of project.

The electrolyser considered for this economic analysis is the AEL given that it is the most utilized commercially available method for industrial-scale electrolysis [63]. The principle of operation of the AEL is depicted in Subsection 1.2.2. Table 3.4 presents all the electrolyser properties and some related economic parameters considered in the present economic assessment study. Note that, according to [63], when considering a 100% electrolyser efficiency, $33.3\ \mathrm{kWh}$ of input electricity is required to produce $1\ \mathrm{kg}$ of $\mathrm{H_2}$. However, since the efficiency of 70% is considered, an input power of $47\ \mathrm{kWh}$ is required to produce $1\ \mathrm{kg}$ of $\mathrm{H_2}$. The project's lifetime is considered $20\ \mathrm{years}$, even though the electrolyser lifetime is assumed to be $10\ \mathrm{years}$ due to its operational hours and stack lifetime.

Table 3.4: AEL properties and economic parameters for the base case.

Properties	Base Value
Stack Lifetime [hours]	83000
% Efficiency	70
Lifetime [years]	10
Input Power [$\mathrm{kWh/kg}$]	47
CAPEX [€/kW]	1600

Regarding the CAPEX estimation, this parameter only considers the initial investment of the electrolyser with a value of 1600 €/kW. No other acquisitions are kept in view in this study, such as compression and storage. On the other hand, the OPEX is assumed to be 3% of the estimated CAPEX, and

this includes costs related to the operation and maintenance of the electrolyser. The electricity price is considered a fixed price over the project lifetime with a value of 0.08 €/kWh. The water price is also assumed as fixed with a value of 1.65 €/m^3. Since the project's lifetime is 20 years and the electrolyser only lasts 10 years, a second electrolyser needs to be purchased. Hence, a new CAPEX must be considered in the year 10 accompanied by its respective OPEX. This new CAPEX is expected to be only 30% of the initial CAPEX in 10 years and the residual value of 25% of the previous eletrolyser is considered.

For the NPV computation, the sales of both $\mathrm{H_2}$ and $\mathrm{O_2}$ are taken into account, having fixed prices over the lifetime of the project. The $\mathrm{H_2}$ is sold with a price of 5 €/kg. Since *per* kg of $\mathrm{H_2}$ produced, 8 kg of $\mathrm{O_2}$ are also produced, the revenues related to $\mathrm{O_2}$ sales are considered to improve the economic profitability of the project. The $\mathrm{O_2}$ is assumed to be sold 90% to both industrial and 10% to medical purposes, with a price of 0.1 €/kg and 0.7 €/kg, respectively. The costs associated with the $\mathrm{O_2}$ and storage cylinders are not considered in the present study and are assumed to be the responsibility of the buyer.

Some of the parameters considered in the calculation of the economic indicators can vary, for such, a sensitivity analysis is effectuated on the NPV, in which the influence of a few variables is analysed. Therefore, it can be determined the weight of each variable in the NPV of the project. The variables contemplated in the sensitivity analysis are presented in Table 3.5, as well as their respective range of variation.

Table 3.5: Variables contemplated in the sensitivity analysis and its respective variation range.

Properties	Base Value	Minimum	Maximum
$\mathrm{H_2}$ selling price [€/kg]	5	1	20
Electricity price [€/kWh]	0.08	0.02	0.5
% Income tax	20	2	25
CAPEX [€/kW]	1600	200	3000
Industrial $\mathrm{O_2}$ selling price [€/kg]	0.1	0	0.5

Apart from the economic impact of the $\mathrm{H_2}$ producer, it is essential to also study the economic impact on the industries when using NG blended with $\mathrm{H_2}$. This study aims to analyse if blending $\mathrm{H_2}$ into the fuel mixture sold to the industry benefits or damages to the companies. It is important to mention that the cost-free $\mathrm{CO_2}$ emissions attributed to each industries will be charged beyond the year 2030 [58]. Therefore, a price per $\mathrm{CO_2}$ license is assumed to be equal to 67 €/$\mathrm{ton_{CO_2}}$ [64]. In addition, the industry is assumed to purchase NG with the price of 120 €/MWh [65] and $\mathrm{H_2}$ with the price mentioned above. However, the prices considered certainly vary overtime, therefore, the effect of its variation is important to be studied. The NG price is varied from 110 €/kWh to 160 €/kWh, the $\mathrm{H_2}$ price from 3.8 €/kg to 5.3 €/kg, and the $\mathrm{CO_2}$ license price from 22 €/$\mathrm{ton_{CO_2}}$ to 247 €/$\mathrm{ton_{CO_2}}$.

Chapter 4

Results and Discussion

Section 4.1 of the present Chapter is the "Model Validation", in which the developed numerical model is validated. Afterwards, Section 4.2 is the "Parametric Study", performed considering several parameters. Then, the "Case of Study" is defined in Section 4.3, which include the power losses study, the influence of blending $\mathrm{H_2}$, an economic assessment from the perspective of the $\mathrm{H_2}$ producer, and a study about the economic impact on the industry.

4.1 Model Validation

In the present Subsection, the model developed in MATLAB-Simulink is validated through a comparison with the work done by Schouten *et al.* in 2004 [37]. Particularly, the results regarding the pressure drop inside the pipeline obtained with the model are compared for a practical example.

The practical example consists of a pipeline with $90\ \mathrm{km}$ and a hydraulic diameter of $1.04\ \mathrm{m}$. The considered mixtures are a lean gas with the composition referred in [37] as well as the same lean gas mixed with $25\%_{\mathrm{mol}}$ of $\mathrm{H_2}$. The simulations are conducted with the data according to the mentioned work, which is summarized in Table 4.1. The schematic representation of the model is depicted in Figure 4.1.

Table 4.1: Validation data from [37].

T [K]	p [MPa]	$\varepsilon \cdot 10^{-6}$ [m]	$\mu \cdot 10^{-6}$ [Pa · s]	Q [$\mathrm{m^3/s}$]
280	6.5	12	12	425

The results obtained are presented in Table 4.2. It is important to emphasize that these simulations were performed with the same amount of gas being transported within the two gaseous mixtures on a volumetric basis.

Table 4.2: Pressure drop on the transmission of NG mixture and blended with $25\%_{\mathrm{mol}}$ of $\mathrm{H_2}$ on the same volumetric basis, in pipeline with $90\ \mathrm{km}$, hydraulic diameter of $1.04\ \mathrm{m}$, and data from Table 4.1.

	$\mathrm{p_2}$ [MPa]	$\mathrm{p_3}$ [MPa]	Pressure drop [MPa]	Pressure drop from [37] [MPa]
100% Mixture of [37]	7.692	6.5	1.192	1.190
75% Mixture of [37] + 25% $\mathrm{H_2}$	7.487	6.5	0.987	0.990

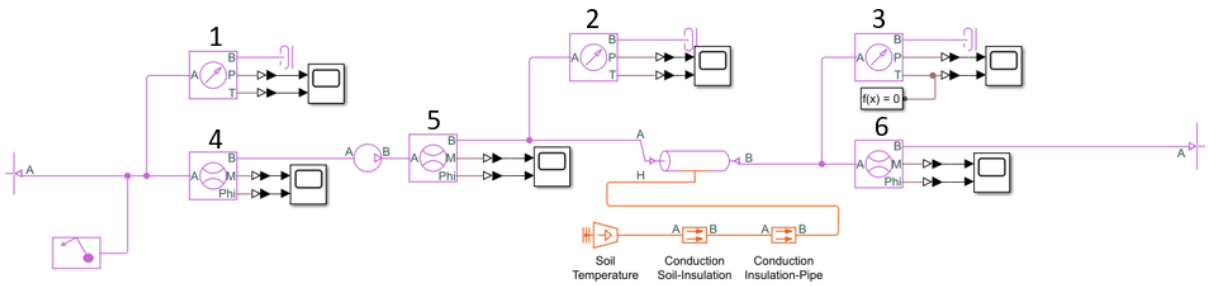

Figure 4.1: Schematic of the simplified model in MATLAB-Simulink with sensors enumerated.

For both transmission of NG and NG blended with $25\%_{\mathrm{mol}}$ of $\mathrm{H_2}$, the pressure drops computed through the measurements effectuated by Sensors 2 and 3 are similar to the values obtained in [37], which demonstrates a good agreement between the results of the developed model and the ones of considered work. Thusly, the developed model is then concluded to be validated.

On the other hand, the simulations are conducted considering the same amount of gas being transported on an energy basis instead of on a volumetric basis, since this is considered in the next studies. Therefore, the results of Table 4.3 are attained.

Table 4.3: Pressure drop on the transmission of NG mixture and blended with $25\%_{\mathrm{mol}}$ of $\mathrm{H_2}$ on the same energy basis, in pipeline with $90\ \mathrm{km}$, hydraulic diameter of $1.04\ \mathrm{m}$, and data from Table 4.1.

	$\mathrm{p_2}$ [MPa]	$\mathrm{p_3}$ [MPa]	Pressure drop [MPa]
100% Mixture of [37]	7.692	6.5	1.192
75% Mixture of [37] + 25% $\mathrm{H_2}$	7.917	6.5	1.417

The pressure drops are larger for the case of the admixture of NG and $\mathrm{H_2}$ compared to the case of only NG, as also concluded in [37]. Therefore, the pressure drop in the pipelines is lesser in the case of NG than in the mixture containing $\mathrm{H_2}$ when the same gas quantity is transported on an energy basis, however it is greater on a volumetric basis. This occurs since, when transporting the same gas quantity with $\mathrm{H_2}$ on a volumetric basis, the correspondent mass flow rate is inferior than when transporting the same gas quantity with $\mathrm{H_2}$ on an energy basis, leading to a lower pressure drop. On the other side, when comparing the case of transporting only NG with the case of the same gas quantity of NG and $\mathrm{H_2}$ on an energy basis, despite the mass flow rate being superior transporting only NG, due to the different inherent gas properties, as it is discussed further, the pressure drop is superior for the case with $\mathrm{H_2}$.

Furthermore, the power of gas flow can also be measured through the appropriate sensors placed in the model (Sensors 4, 5, and 6 of Figure 4.1). Thus, it is possible to compute the efficiency and power losses of the transmission system. For such, the case of transporting the same amount of gas on an energy basis is once more considered, and the results of Table 4.4 are obtained.

By observing the results of Table 4.4, the efficiency in the transmission computed through the power measurements is lower for the case with $\mathrm{H_2}$ blended in the mixture than in the case without. This means that the transmission of the admixture of NG with $\mathrm{H_2}$ has more power losses associated. When both Table 4.3 and Table 4.4 are compared, it can also be discerned that larger pressure drops correspond

Table 4.4: Power losses on the transmission of NG mixture and blended with $25\%_{\mathrm{mol}}$ of $\mathrm{H_2}$ on the same energy basis, in pipeline with $90\ \mathrm{km}$, hydraulic diameter of $1.04\ \mathrm{m}$, and data from Table 4.1.

	% Efficiency	% Power losses
100% Mixture of [37]	86.77	13.23
75% Mixture of [37] + 25% $\mathrm{H_2}$	83.75	16.25

to higher power losses in the pipeline.

4.2 Parametric Study

A parametric study is conducted considering the model used in the previous Subsection and default parameters similar to the case of study. The parameters under study, such as percentage of $\mathrm{H_2}$ in the mixture, hydraulic diameter, mass flow rate, length, and roughness, are varied in the present study. The base values of the parameters are presented in Table 4.5, and each one of them is varied in the respective study while the others are kept at its base value. The fixed parameters that are out of scope in the present parametric study are briefly summarized in Table 4.6, and they are similar to the ones of the case of study.

Table 4.5: Base values of the parameters considered in the parametric study.

D_{hyd} [m]	$\dot{m}$ [kg/s]	L [km]	$\varepsilon \cdot 10^{-6}$ [m]
0.7	100	90	50

Table 4.6: Fixed parameters in the parametric study.

T [K]	p [MPa]	$\mathrm{T_{soil}}$ [K]	k_{soil} [$\mathrm{W/m \cdot K}$]	k_{insul} [$\mathrm{W/m \cdot K}$]
300	8.0	293.15	1.56	0.3175

The objective of this analysis is to acknowledge the influence of each parameter on the power loss inside the pipeline. Firstly, the effect of assuming NG composed of 100% $\mathrm{CH_4}$ is studied as well as the effect of mixing several percentages of $\mathrm{H_2}$. Afterwards, the parameters regarded in this study include the pipeline's hydraulic diameter, incoming mass flow rate, length, and roughness. From this point forward, all the studies are effectuated on the same energy basis. This parametric study is relevant since it is conducted in the simplified model of the RNTGN, thus, its conclusions are the base for understanding the results later obtained in the more complex case of study.

4.2.1 Assumption of 100% Methane

As previously mentioned, the NG is assumed to be composed of 100% $\mathrm{CH_4}$ in the computations related to the case of study. Therefore, it is pivotal to understand the impacts of using this simplification. For such, the power loss result is obtained for the NG mixture considered in Subsection 4.1 and for this

approximation, through the measurements effectuated by Power Sensors 5 and 6. Hence, the results are presented in Table 4.7.

Table 4.7: Comparison between mixture used in Subsection 4.1 and assumption of $100\%\ \mathrm{CH_4}$, considering the data from Tables 4.5 and 4.6.

	% Efficiency	% Power losses
Mixture of 4.1	95.35	4.65
$100\%\ \mathrm{CH_4}$	95.34	4.66

Through the analysis of Table 4.7, it can be discerned that the power loss using this approximation differs approximately 0.01% from the value obtained with the more complex NG mixture. Therefore, this simplification is concluded to have almost no effect on the obtained results, and it is considered in the next studies.

4.2.2 Percentages of Hydrogen

As previously highlighted, one of the main objectives of the present work is to contribute to the investigation of the viability of injecting $\mathrm{H_2}$ in the RNTGN, with the aim of slowly start decarbonising the Portuguese network. Since the case of study contemplates the study of the effect of blending $\mathrm{H_2}$ in the mixture, it is important to study the influence of this parameter on the power losses associated with its transmission. For such, a parametric study about the volumetric percentages of injected $\mathrm{H_2}$ is performed in the simplified model, exploring $5\%_{\mathrm{vol}}$, $10\%_{\mathrm{vol}}$, and $20\%_{\mathrm{vol}}$ of $\mathrm{H_2}$, which are the percentages investigated in the case of study. The attained results are presented in Table 4.8 and in the plot of Figure 4.2.

Table 4.8: Influence of percentage of $\mathrm{H_2}$ present in the mixture on the percentage of power loss associated with its transmission, considering the data from Tables 4.5 and 4.6.

	% Efficiency	% Power losses
$100\%\ \mathrm{CH_4}$	95.34	4.66
$95\%\ \mathrm{CH_4}$ + $5\%\ \mathrm{H_2}$	95.02	4.98
$90\%\ \mathrm{CH_4}$ + $10\%\ \mathrm{H_2}$	94.67	5.33
$80\%\ \mathrm{CH_4}$ + $20\%\ \mathrm{H_2}$	93.85	6.15

Observing the results of Table 4.8, the transmission efficiency decreases when the percentage of blended $\mathrm{H_2}$ increases. This translates on the percentage of power losses increasing as the percentage of blended $\mathrm{H_2}$ also increases. This increase of power losses when increasing the percentage of blended $\mathrm{H_2}$ is in line with the conclusions already provided in Section 4.1 in the case of the same amount of gas is transported on an energy basis.

Moreover, the plot of Figure 4.2 evidences a linear trend between both values. When a linear regression is executed, the correspondent coefficient of determination R^2 is relatively high with a value of 0.997. Since R^2 is the variation proportion in the dependent variable that can be predicted from the independent variable, one can conclude that the power losses are proportional to the percentage of $\mathrm{H_2}$.

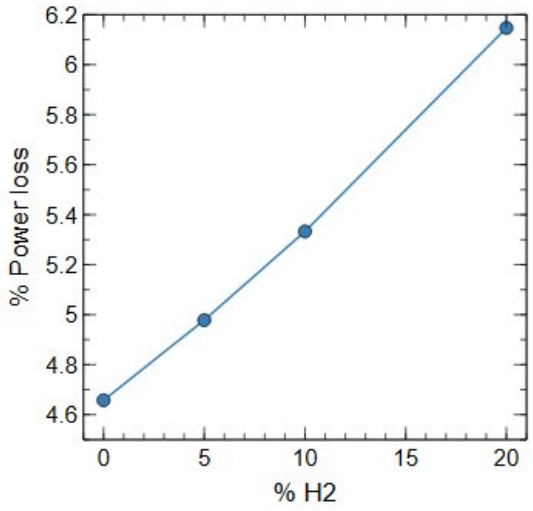

Figure 4.2: Percentage of power losses as function of the percentage of $\mathrm{H_2}$ blended, considering the data from Tables 4.5 and 4.6.

From this point further, when it is mentioned that a certain percentage of $\mathrm{H_2}$ is blended into the mixture, it always refers to the percentage in volume.

4.2.3 Hydraulic Diameter

As presented in Table 3.1 of Subsection 3.1.1, the RNTGN is composed of various segments that have different hydraulic diameters. Since the results of the power losses in the case of study consider all these hydraulic diameters, it is of extreme importance to investigate the influence of this parameter on the simplified model. Therefore, the parameter under study in this Subsection is the pipe's hydraulic diameter. Particularly, the values considered are $0.5\ \mathrm{m}$, $0.7\ \mathrm{m}$, $0.9\ \mathrm{m}$, and $1.1\ \mathrm{m}$. The results are obtained for $\mathrm{CH_4}$, as well as its admixture with 20% of $\mathrm{H_2}$ and they are presented in Table 4.9 and Table 4.10, respectively, and in both plots of Figure 4.3.

Table 4.9: Influence of hydraulic diameter on the transmission of $100\%\ \mathrm{CH_4}$, considering the remaining data from Table 4.5 and data from Table 4.6.

D_{hyd} [m]	% Efficiency	% Power losses
0.5	91.86	8.14
0.7	95.34	4.66
0.9	96.09	3.91
1.1	96.19	3.81

Firstly, it can be denoted that there are smaller power losses with larger diameters, and this occurrence is verified in both Tables 4.9 and 4.10. When observing plot (a) of Figure 4.3, it is clear the considerable decrease of power losses when the hydraulic diameter increases, but always bearing in mind that the power losses are superior when the mixture contains $\mathrm{H_2}$, as verified in the Subsection 4.2.2. The explanation for the abrupt behaviour can be justified when analysing the influence of the

Table 4.10: Influence of hydraulic diameter on the transmission of $80\%\ \mathrm{CH_4}$ with $20\%\ \mathrm{H_2}$, considering the remaining data from Table 4.5 and data from Table 4.6.

D_{hyd} [m]	% Efficiency	% Power losses
0.5	89.42	10.58
0.7	93.85	6.15
0.9	94.88	5.12
1.1	95.02	4.98

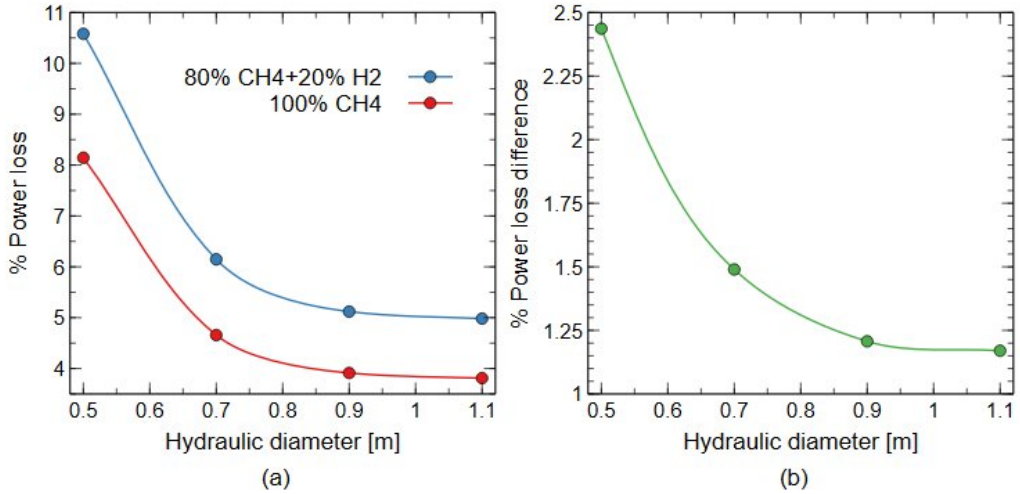

Figure 4.3: Percentage of power loss as a function of the hydraulic diameter [m] for $100\%\ \mathrm{CH_4}$ (red) and $80\%\ \mathrm{CH_4}$ with $20\%\ \mathrm{H_2}$ (blue), and the difference between both values also as a function of hydraulic diameter [m], considering the remaining data from Table 4.5 and data from Table 4.6.

hydraulic diameter on pressure drops due to viscous friction. Particularly, Equations (2.6a) and (2.6b) establish that the pressure drops due to viscous friction are inversely proportional to D_{hyd}^5. Given that the pressure drop due to viscous friction is a strong component that influences the power losses, this relationship highly affects the results. Finally, through observation of plot (b) of Figure 4.3, the difference between the power losses of the mixture with only $\mathrm{CH_4}$ and with $\mathrm{H_2}$ decreases with the increase of the hydraulic diameter.

4.2.4 Mass Flow Rate

The developed numerical model is able to receive as an input different mass flow rates. Actually, since the RNTGN transports the NG to feed the demand to the industry, these industries may need different mass flow rates in various circumstances to satisfy their necessities. Therefore, the following parameter to be analysed is the mass flow rate coming into the pipe. Since the computations are performed in the same amount of gas being transported on an energy basis, the $\mathrm{CH_4}$ mass flow rate differs from the mass flow rate of the admixture of $\mathrm{CH_4}$ with $20\%\ \mathrm{H_2}$. Therefore, the values of $\mathrm{CH_4}$ mass flow rate – equivalent mass flow rate – considered are $25\ \mathrm{kg/s}$, $50\ \mathrm{kg/s}$, $80\ \mathrm{kg/s}$, $100\ \mathrm{kg/s}$, and $150\ \mathrm{kg/s}$, as well as the corresponding values of the mass flow rate of the admixture with $\mathrm{H_2}$. Thus, the obtained

results are presented in Table 4.11, Table 4.12, and in the plot of Figure 4.4.

Table 4.11: Influence of equivalent mass flow rate on the transmission of $100\%\ \mathrm{CH_4}$, considering the remaining data from Table 4.5 and data from Table 4.6.

$\dot{m}_{\mathrm{eqv}}$ [$\mathrm{kg/s}$]	% Efficiency	% Power losses
25	97.41	2.59
50	96.96	3.04
80	96.06	3.94
100	95.34	4.66
150	93.38	6.62

Table 4.12: Influence of equivalent mass flow rate on the transmission of $80\%\ \mathrm{CH_4}$ with $20\%\ \mathrm{H_2}$, considering the remaining data from Table 4.5 and data from Table 4.6.

$\dot{m}_{\mathrm{eqv}}$ [$\mathrm{kg/s}$]	% Efficiency	% Power losses
25	96.84	3.16
50	96.13	3.87
80	94.83	5.17
100	93.85	6.15
150	91.25	8.75

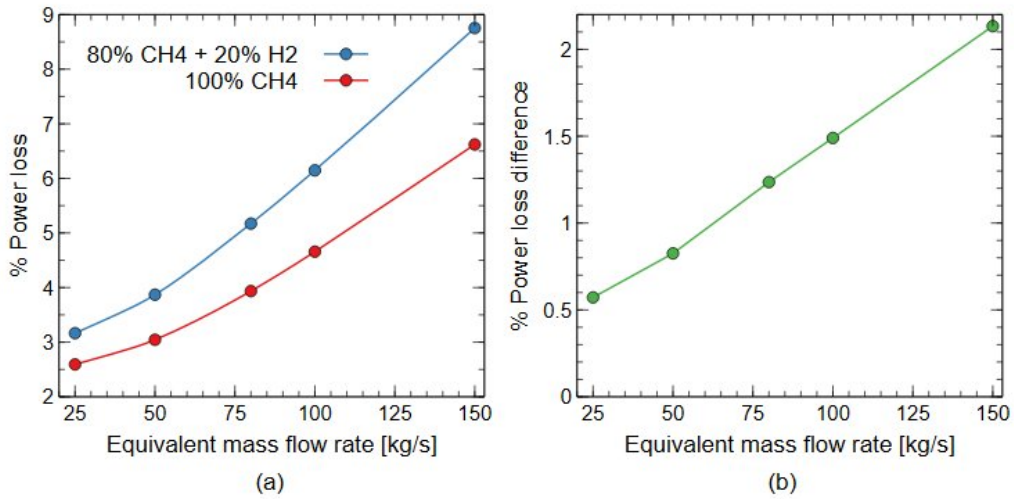

Figure 4.4: Percentage of power loss as a function of the equivalent mass flow rate [$\mathrm{kg/s}$] for $100\%\ \mathrm{CH_4}$ (red) and $80\%\ \mathrm{CH_4}$ with $20\%\ \mathrm{H_2}$ (blue), and the difference between both values also as a function of the equivalent mass flow rate [$\mathrm{kg/s}$], considering the remaining data from Table 4.5 and data from Table 4.6.

First of all, the power losses are demonstrated to rise when the equivalent mass flow rate increases in Tables 4.11 and 4.12. This statement can be notably observed in plot (a) of Figure 4.4, where an approximate quadratic trend can be detected. In fact, these results can be explained through Equations (2.6a) and (2.6b) since the pressure drop due to viscous friction is proportional to the square of the mass flow rate entering the pipeline. Once again, the power losses are superior in the case of the mixture with $\mathrm{H_2}$, which agrees with the results of Subsection 4.2.2. Finally, the difference between both power losses

seems to increase almost linearly with the increase of the equivalent mass flow rate in plot (b) of Figure 4.4.

4.2.5 Length

The RNTGN is constituted of segments with different characteristics, including the pipeline's length. Hence, the results of the case of study are affected by the length of the pipeline included in the gas trajectory and it is relevant to understand the impact of this parameter on the simplified model. Therefore, the effect of altering the pipeline's length is examined in the present parametric study. The values $50\ \mathrm{km}$, $90\ \mathrm{km}$, and $125\ \mathrm{km}$ are taken into account in this study. Hence, the attained results are showcased in Table 4.13 for $\mathrm{CH_4}$ transmission, in Table 4.14 for the admixture with $\mathrm{H_2}$, and in the plots of Figure 4.5.

Table 4.13: Influence of pipeline's length on the transmission of $100\%\ \mathrm{CH_4}$, considering the remaining data from Table 4.5 and data from Table 4.6.

L [km]	% Efficiency	% Power losses
50	96.85	3.15
90	95.34	4.66
125	94.29	5.71

Table 4.14: Influence of pipeline's length on the transmission of $80\%\ \mathrm{CH_4}$ with $20\%\ \mathrm{H_2}$, considering the remaining data from Table 4.5 and data from Table 4.6.

L [km]	% Efficiency	% Power losses
50	95.94	4.06
90	93.85	6.15
125	92.38	7.62

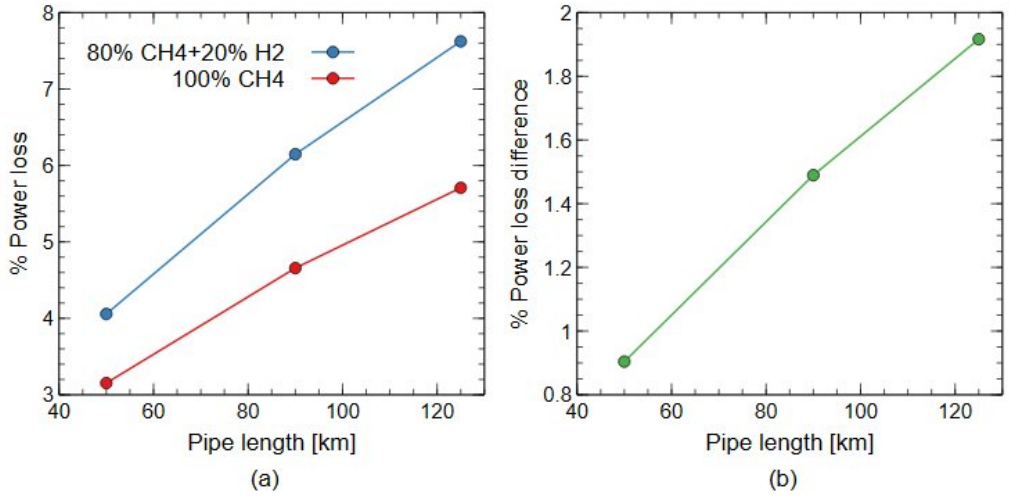

Figure 4.5: Percentage of power loss as a function of the pipeline's length [km] for $100\%\ \mathrm{CH_4}$ (red) and $80\%\ \mathrm{CH_4}$ with $20\%\ \mathrm{H_2}$ (blue), and the difference between both values also as a function of the pipeline's length [km], considering the remaining data from Table 4.5 and data from Table 4.6.

The extending of pipeline's length is denoted to increase the power losses associated with the gas transmission. Once more, this trend is observable in both Tables 4.13 and 4.14, with the power losses related with the presence of $\mathrm{H_2}$ being higher, assenting with the results of Subsection 4.2.2. When analysing plot (a) of Figure 4.5, the power loss as a function of the pipe length exhibits a linear trend. The coefficients of determination R^2 are 0.9959 and 0.9963, for the case with only $\mathrm{CH_4}$ and with $\mathrm{H_2}$, respectively, when a linear regression is effectuated. This trend can be enlightened by Equations (2.6a) and (2.6b), where it can be verified that the pressure drop due to viscous friction is proportional to the pipeline's length. Plot (b) of Figure 4.5 also evidences a linear trend on the difference of both power losses as a function of the pipe length.

4.2.6 Roughness

Despite the internal surface absolute roughness being considered always the same value in all the RNTGN in the developed computational tool, it is an important parameter in fluid flow inside a pipeline. Therefore, the influence of this parameter is contemplated on the simplified model. Hence, the values taken into consideration on this study are $0.01\ \mathrm{mm}$, $0.03\ \mathrm{mm}$, and $0.05\ \mathrm{mm}$. The results are presented in Table 4.15 for $\mathrm{CH_4}$ transmission, in Table 4.16 for the admixture with $\mathrm{H_2}$, and in the plots of Figure 4.6.

Table 4.15: Influence of roughness on the transmission of $100\%\ \mathrm{CH_4}$, considering the remaining data from Table 4.5 and data from Table 4.6.

$\varepsilon \cdot 10^{-6}$ [m]	% Efficiency	% Power losses
10	95.60	4.40
30	95.44	4.56
50	95.34	4.66

Table 4.16: Influence of roughness on the transmission of of $80\%\ \mathrm{CH_4}$ with $20\%\ \mathrm{H_2}$, considering the remaining data from Table 4.5 and data from Table 4.6.

$\varepsilon \cdot 10^{-6}$ [m]	% Efficiency	% Power losses
10	94.21	5.79
30	93.99	6.01
50	93.85	6.15

From Tables 4.15 and 4.16, the increase of the internal surface absolute roughness increases the percentage of power loss. Once more, the power losses are superior in the case of the transmission of the mixture with $\mathrm{H_2}$, agreeing with Section 4.1. In plot (a) of Figure 4.6, the trend between the percentage of power loss and roughness is depicted and in line Equations (2.6a), (2.6b), (2.7a), and (2.7b). The roughness has a minor influence on the power loss result. For example, a decrease of 80% from the roughness base value, it only results on a decrease of approximately 5.6% on the power loss, for the NG transmission. Finally, plot (b) of Figure 4.6 portrays the correlation between the difference of power losses between the case with and without $\mathrm{H_2}$, and the roughness.

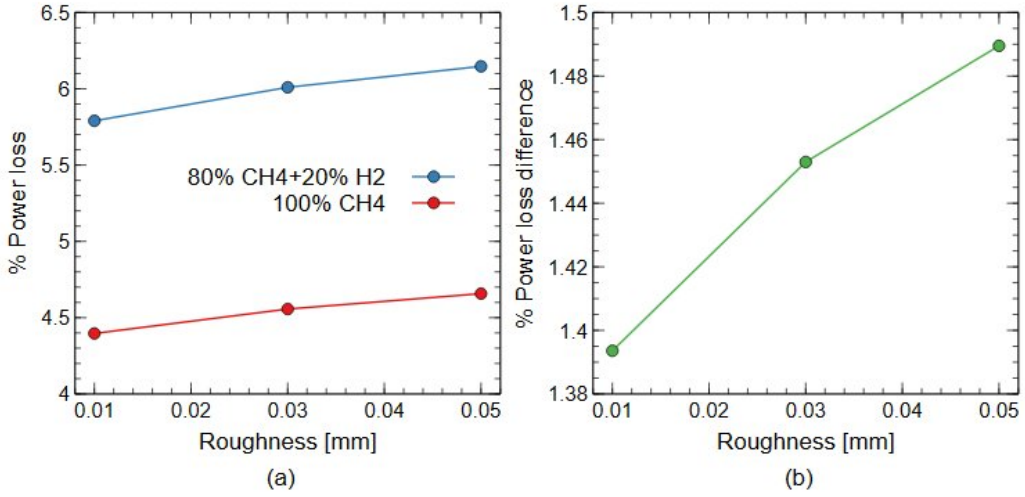

Figure 4.6: Percentage of power loss as a function of the roughness [mm] for 100% $\mathrm{CH_4}$ (red) and 80% $\mathrm{CH_4}$ with 20% $\mathrm{H_2}$ (blue), and the difference between both values also as a function of the roughness [mm], considering the remaining data from Table 4.5 and data from Table 4.6.

As a final point, the conclusions from these four parametric studies applied in the simplified model are essential to later understand the results obtained for the more complex case of study in Section 4.3.

4.3 Case of Study

The case of study consists of the definition of several supply scenarios within the Portuguese context, as explained in Subsection 3.1.1. The main objective is to determine the percentage of power losses associated with the transmission of the mass flow rate through the trajectory inside the pipelines until arriving at each industry. This case of study is considered in the four studies that are performed next, such as the power losses study, the influence of blending hydrogen, economic assessment of hydrogen production, and economic impact on the industry.

4.3.1 Power Losses Study

The first study performed by employing the developed computational tool in MATLAB-Simulink for the case of study is a power losses study. Briefly, the energy required to feed the Portuguese industrial consumers is computed through the list presented in Appendix A.1 [58]. Also, as verified previously in Subsection 4.2.1, the employment of the assumption that NG is composed by 100% $\mathrm{CH_4}$ is considered reasonable. Therefore, whenever NG is mentioned in this study, it refers to this approximation. Afterwards, it is computed the total NG mass flow rate required to feed those necessities, and this value is the input of the system at LNG Terminal at Sines. While the NG is transported through the trajectory of the various defined segments, the industries are being supplied by geographical order. At the end of the final segment, all the NG mass flow rates should already had been distributed to all companies. The methodology behind this tool is described in more detail in Subsection 3.1.1.

The power losses study is conducted for all scenarios explained, and each one requires a specific energy to feed the demand associated, and therefore a different power loss associated. For example, for Scenario (A), an annual energy supply of $41.97\ \mathrm{TWh}$ is required to satisfy the demand of the Portuguese industrial consumers. This energy translates on a NG mass flow rate of $95.74\ \mathrm{kg/s}$ that is provided from the LNG Terminal at Sines. This mass flow rate is then transported through the segments and the respective needed quantity is delivered to each industry along the way. The Reynolds number of the flow circulating inside the pipeline is determined through Equation (2.5a) and it is concluded to be equal to $1.3 \cdot 10^7$, confirming that this flow is in the turbulent regime.

Regarding Scenario (B), the Portuguese industry stands in need for the same energy, and the energy to be exported is an extra $4.20\ \mathrm{TWh}$. For instance, the mass flow rate to be supplied to the industry amounts to $95.74\ \mathrm{kg/s}$ and the mass flow rate to be exported to Spain of $9.57\ \mathrm{kg/s}$. As previously mentioned, this scenario contemplates two courses of exportation among three possibilities, which include the exportation fully through Valença do Minho (B.1), fully through Campo Maior (B.2), and divided through both at the same time (B.3). In practical terms, the total NG mass flow rate is inputted at Sines, as it is in Scenario (A), and it is transported through the segments distributing NG to each industry along the course. Depending on the course of exportation, the remaining mass flow rate at the end of the segment Cantanhede - Valença do Minho (B.1) or at the end of Bidoeira - Campo Maior (B.2) , or even half at both (B.3), is the value of mass flow rate to be exported to Spain.

For Scenario (C), the caverns of Carriço Underground Gas Storage are filled as the same time as the Portuguese industrial consumers are fed, all with NG supplied from LNG Terminal at Sines. However, the caverns' maximum injection capability is restrained to $2\ \mathrm{Mm^3/day}$ [16], which limits the amount of NG that can be introduced *per* second (C.1). This scenario also contemplates the hypothetical case of this injection capability being doubled up to $4\ \mathrm{Mm^3/day}$ (C.2). Essentially, the required NG mass flow rate, which include the Portuguese industrial consumers and the caverns, is inputted in the LNG Terminal at Sines. Once again, it is transported along the RNTGN while being delivered to the industries, and to the caverns of Carriço when passing through the segment Bidoeira-Figueira da Foz.

Furthermore, Scenario (D) comprises the extraction of NG from Carriço Underground Gas Storage. Since the caverns' maximum extraction capability is limited to $7.2\ \mathrm{Mm^3/day}$ [16], which is insufficient to satisfy the whole demand, the supply from LNG Terminal at Sines is necessary to provide the remaining quantity. Therefore, Scenario (D) requires the NG mass flow rate as an input at Carriço as well as at Sines. Particularly, the mass flow rate input from Sines starts being delivered to the industries supplied from the segment Sines – Setúbal and the following, until arriving to Bidoeira. On the other hand, a part of mass flow rate coming out of Carriço goes to Figueira da Foz direction to feed their nearby industries, and the other part goes to Bidoeira. Hence, the remaining from both inputs, that has not been yet delivered to its industry, assembles and continues its trajectory to Campo Maior direction and going north to Valença do Minho, to gradually be supplied.

Hence, the aforementioned scenarios are applied in the developed computational tool and the results of the power losses associated to the NG transmission are obtained. These results are presented in Table 4.17.

Table 4.17: Power losses results with regard to NG transmission for all scenarios.

	(A)	(B.1)	(B.2)	(B.3)	(C.1)	(C.2)	(D)
% Power losses	4.21	5.27	5.23	5.18	6.00	7.98	3.22

Firstly, the power loss associated with the NG transmission of Scenario (A) is 4.21%. Note that Scenario (A) solely considers the NG mass flow rate required to feed the Portuguese industrial consumers.

Secondly, the power losses of Scenarios (B.1), (B.2), and (B.3) are 5.27%, 5.23%, and 5.18%, respectively. It is important to recall these scenarios involve the supply of the Portuguese industrial consumers as well as exportation to Spain. Concretely, Scenario (B.1) contemplates the exportation through Valença do Minho, Scenario (B.2) through Campo Maior, and Scenario (B.3) through both locations at the same time. Since the mass flow rate is inputted in the LNG Terminal at Sines for these scenarios, the distance from Sines to these exportation locations should be emphasised. In fact, Campo Maior is closer to Sines compared to Valença do Minho, which is located in the north extremity of Portugal. As verified in the parametric study of Subsection 4.2.5, the power losses are verified to increase when the pipeline length is longer. Thereafter, this explains the power losses of Scenario (B.1) being 5.27%, larger than the 5.23% of Scenario (B.2). Besides, as seen in the parametric study of Subsection 4.2.4, the increase of the mass flow rate entering the pipeline implies an increase of the associated power losses. Particularly for the simplified model considered in the parametric studies, the power losses are acknowledged to be approximately proportional to the length and to the square of mass flow rate, showing a dominance of the mass flow rate effect on the power losses over the pipeline extension. This dominance explains the power loss result for the Scenario (B.3) of 5.18%, due to the fact that this scenario considers the division of the mass flow rate to be exported into both locations. Therefore, there is less quantity of mass flow rate going through the pipeline segments to each direction, despite the distance from Sines to Valença do Minho being superior. Hence, Scenario (B.3) is the most interesting exportation scenario, since the power loss associated is the lowest among the three exportation options.

Thirdly, Scenarios (C.1) and (C.2) present power losses of 6.00% and 7.98%. It must be recalled that Scenario (C.1) comprises the Portuguese industry as well as the filling of the caverns of Carriço Underground Storage with the maximum allowed mass flow rate at the present time, and that Scenario (C.2) contemplates the same industry and the hypothetical case of doubling the maximum allowed mass flow rate to fill those salt caverns. In terms of travelled distances inside the pipelines, both Scenarios (C.1) and (C.2) are similar, and the only difference relies on the amount of NG mass flow rate being transported inside the pipelines. Due to the specific situation of each scenario, Scenario (C.2) requires more mass flow rate circulating inside the RNTGN than Scenario (C.1). Since the power loss of Scenario (C.2) – 7.98% – is higher than the power loss of Scenario (C.1) – 6.00% –, it corroborates with the conclusions of the parametric study of Subsection 4.2.4, which states that a superior mass flow rate circulating inside a pipe has a larger power loss related to its transmission.

Regarding Scenario (D), the related power losses are 3.22%. Scenario (D) uses the NG stored inside the caverns of Carriço Underground Storage to supply the industry, with support from LNG Terminal at Sines, due to the maximum allowed mass flow rate to be extracted from the caverns at the present time.

This scenario presents the lowest percentage of power loss of all the considered scenarios, which is attributable to two contributions. To begin with, there is less distance to be travelled by the NG inside the pipelines considering that there are two sources of NG input into the network (Sines and Carriço). Moreover, there is less mass flow rate in the segments for the same reason. Therefore, the power loss associated with this scenario is the lowest.

As a result, one can conclude that it is decidedly advantageous to use the NG stored inside the salt caverns of Carriço Underground Storage to feed the demand necessities of the Portuguese industrial sector in terms of power losses. However, as seen in Scenarios (C.1) and (C.2), the fill of these caverns has its own associated power losses. Therefore, a beneficial strategy could be to fill in the caverns in periods where the industrial demand is not at its peak, for example, at night. Another possible strategy to better exploit the results could be to build more salt caverns distributed along the territory. This would have less power losses associated with both its filling and its usage to satisfy the NG demand from the industry. Nonetheless, it cannot be overlooked the specific geological structure that is necessary to built such infrastructures, as explained in Subsection 1.2.1. The construction of new caverns also evolve the consideration of environmental regulations to deposit the salt extracted to empty the caverns. For example, Figure 1.7 of Subsection 1.2.1 shows that the Monte Real salt structure has capability of spreading more caverns along the littoral coast, which would be beneficial to employ this strategy.

4.3.2 Influence of Blending Hydrogen

Since one of the main objectives of the present Dissertation is to understand the effects of injecting $\mathrm{H_2}$ in the NG mixture on the power losses associated with its transmission in the RNTGN, the computational tool also computes the results for several percentages of $\mathrm{H_2}$. Further, these results are compared to the case of transmission of NG without $\mathrm{H_2}$ in the mixture.

Hence, the influence of blending several percentages of $\mathrm{H_2}$ into NG (5%, 10%, and 20% of $\mathrm{H_2}$) on the power losses is contemplated in the present Subsection. The mixture properties for each composition are presented in Table 3.3 of Subsection 3.1.2. The same scenarios are considered in this study. First of all, the Portuguese industrial consumers still require the same amount of energy. However, since the LHV of $\mathrm{H_2}$ is higher than the LHV of $\mathrm{CH_4}$, the required mass flow rate is inferior compared to the case of transporting only NG.

Results for Scenario (A)

At first, the results are only obtained for Scenario (A) for the three $\mathrm{H_2}$ percentages. Scenario (A) included the supply of the Portuguese industrial consumers with mass flow rate from LNG Terminal at Sines. The case of Subsection 4.3.1, which regards the transmission of NG without any $\mathrm{H_2}$, requires a mass flow rate of $95.74\ \mathrm{kg/s}$. However, as previously explained, different mass flow rates are required to satisfy the same industry demand. Concretely, for Scenario (A), a mass flow rate of $94.89\ \mathrm{kg/s}$, $93.97\ \mathrm{kg/s}$, and $91.90\ \mathrm{kg/s}$ is necessary for 5%, 10%, and 20% of $\mathrm{H_2}$, respectively, since the same amount of gas is being transported on an energy basis. Accordingly, the results of Table 4.18 are attained using

the developed computational tool.

Table 4.18: Power losses results for Scenario (A) with regard to transmission of the admixture with several percentages of H_2.

	100% NG	95% NG + 5% H_2	90% NG + 10% H_2	80% NG + 20% H_2
% Power losses	4.21	4.86	5.44	6.83

As also acknowledged in Subsection 4.2.2, the higher the percentage of H_2 in the mixture, more power losses are associated with its transmission. Despite the mass flow rate being inferior when there is more percentage of H_2 present in the mixture, the power losses associated with its transmission are increasing, as also occurred in Subsection 4.2.2. This increase of power loss can be explained by the change of the mixture properties when adding more H_2. Particularly, the mixture density is severely affected by the H_2 addition and it decreases considerably, as can be observed in Table 3.3 of Subsection 3.1.2. When the mixture density decreases, the pressure drop due to viscous friction increases, as seen in Equations (2.5a) and (2.5b). Given that the power loss is highly influenced by the pressure drop due to viscous friction, as established in Section 4.1, the power loss also increases when the pressure drop does, justifying the obtained results for Scenario (A). Another explanation relies on power losses also being influenced by the losses due to heat transfer along the pipe. Particularly, when H_2 is added, the thermal conductivity of the mixture increases considerably, as can be observed in Table 3.3 of Subsection 3.1.2. Since heat conduction contributes for the heat transfer along the pipe, through Equation (2.9), it can be established that higher thermal conductivity results in larger heat transfer. Therefore, this also contributes to the larger power losses when a higher percentage of H_2 is present in the mixture.

Correlation for Power Losses

When analysing the obtained results from Scenario (A), they evidence a linear trend, as also occurred in the parametric study of Subsection 4.2.2, with a coefficient of determination R^2 of 0.999. Thus, a linear regression can be computed to estimate the percentage of power losses obtained by transporting mixtures with different percentages of H_2. The plot of Figure 4.7 shows the performed linear regression and the developed correlation to calculate the power losses, which is also written in Equation (4.1), for a percentage of hydrogen between 0 - 20% present in the mixture.

$$\%\text{Power losses} = 0.1295 \cdot \%H_2 + 4.21 \tag{4.1}$$

In addition, this correlation can be extended to be also employed to estimate the power losses for the other scenarios. For such, the only modification that needs to be made is the replacement of the value 4.21%, which is the value of the power loss transporting only NG for Scenario (A), by the value of the power loss transporting only NG in the respective scenario, displayed in Table 4.17. The general correlation is written in Equation (4.2), where b is the percentage of power loss of transporting only NG for the respective scenario.

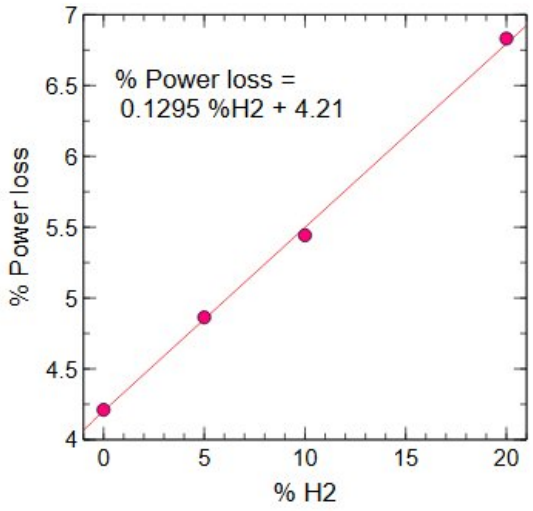

Figure 4.7: Linear regression for percentage of power loss as a function of the percentage of $\mathrm{H_2}$ in the mixture for Scenario (A).

$$\%\text{Power losses} = 0.1295 \cdot \%\mathrm{H_2} + \mathrm{b} \tag{4.2}$$

Accordingly, Table 4.19 shows all the obtained power losses computed through this correlation for every scenario, for a percentage of hydrogen between 0-20% present in the mixture.

Table 4.19: Power losses of transmission of several percentages of $\mathrm{H_2}$ for all scenarios estimated through Equation (4.2).

	(A)	(B.1)	(B.2)	(B.3)	(C.1)	(C.2)	(D)
100% NG	4.21	5.27	5.23	5.18	6.00	7.98	3.22
95% NG + 5% $\mathrm{H_2}$	4.86	5.92	5.88	5.83	6.64	8.63	3.87
90% NG + 10% $\mathrm{H_2}$	5.44	6.57	6.53	6.48	7.29	9.27	4.52
80% NG + 20% $\mathrm{H_2}$	6.83	7.86	7.82	7.77	8.59	10.57	5.81

4.3.3 Economic Assessment of Hydrogen Production

Since one of the objectives of this Dissertation is to analyse the influence of injecting $\mathrm{H_2}$ on the power losses, it is essential to understand if the project to produce the $\mathrm{H_2}$ to be injected is economically viable. Hence, this Subsection regards an economic assessment about the production of $\mathrm{H_2}$ that is subsequently blended into the NG mixture. The economic assessment regarding the $\mathrm{H_2}$ production project is performed in the perspective of a private $\mathrm{H_2}$ producer. For this study, the electrolyser is located near the LNG Terminal at Sines, therefore, the power losses related to the transmission computed in the previous subsections are taken into consideration. The methodology behind this assessment is described with detail in Section 3.2.

The first economic indicator to be computed is the LCOH, followed by the NPV, IRR, and PBP for

the production of $\mathrm{H_2}$ to feed Scenario (A) with 5% of $\mathrm{H_2}$ present in the mixture. Afterwards, the NPV is calculated for producing the $\mathrm{H_2}$ to supply the demand in all scenarios when transporting a mixture with 5% of $\mathrm{H_2}$. Following that, a sensitivity analysis is performed for the supply of Scenario (A), where several parameters are under study, including the percentage of $\mathrm{H_2}$ blended in the mixture.

Levelised Cost of Hydrogen

The LCOH calculation considered the project's lifetime of $20\ \mathrm{years}$. The CAPEX regarded only the initial investment of the electrolyser, with a value of 1600 €$/\mathrm{kg}$, and an OPEX of 3% of the CAPEX. Since the lifetime of the electrolyser is only $10\ \mathrm{years}$, it is necessary to consider a second CAPEX of the investment of a second eletrolyser. The electricity and water prices are 0.08 €$/\mathrm{kWh}$ and 1.65 €$/m^3$, respectively. All these assumptions are detailedly explained in Section 3.2.

Therefore, the LCOH is computed using Equation (2.14), and a LCOH value of 4.99 €$/\mathrm{kg_{H_2}}$ is determined, for the three $\mathrm{H_2}$ percentages for all scenarios. This computed value is lower than the LCOH determined in [54–56], which evidence that this project may be cost-competitive to produce hydrogen via AEL. Furthermore, the computation results in the same value for all scenarios since the $\mathrm{H_2}$ production cost is proportional to the quantity of $\mathrm{H_2}$ produced. This means that, regardless of existing scenarios with larger power losses associated, and consequently more $\mathrm{H_2}$ in need to be produced to compensate for them, the computed LCOH is still the same since the ratio between the costs of production and the quantity produced is also the same.

Net Present Value, Internal Rate of Return, and Payback Period

First of all, the NPV, IRR, and PBP are only computed for the project of the production of the quantity of $\mathrm{H_2}$ to feed Scenario (A) transporting a mixture with 5% of $\mathrm{H_2}$. Note that the determination of the NPV includes the sales of $\mathrm{H_2}$, industrial $\mathrm{O_2}$, and medical $\mathrm{O_2}$, with prices of 5 €$/\mathrm{kg}$, 0.1 €$/\mathrm{kg}$, and 0.7 €$/\mathrm{kg}$, respectively. Once again, all the simplifications and considerations of this assessment model are explained in Section 3.2.

Therefore, using Equation (2.15), the computed NPV for Scenario (A) with 5% of $\mathrm{H_2}$ is 242.79 M€. This NPV value is positive which characterizes a economically viable project with a good margin of profit. Through Equations (2.16) and (2.17), the IRR is 21% and the PBP is approximately $5\ \mathrm{years}$.

Additionally, the NPV is also computed for the project of producing $\mathrm{H_2}$ to feed all scenarios transporting a mixture containing 5% of $\mathrm{H_2}$, and the results are presented in the bar chart of Figure 4.8.

From the bar chart of Figure 4.8, all the $\mathrm{H_2}$ production projects to supply every scenario, that comprise transporting a mixture with 5% of $\mathrm{H_2}$, have a positive NPV, meaning that all of them are economically viable. Particularly, Scenario (C.2) is the one whose $\mathrm{H_2}$ production project has more associated profitability. This occurs since this scenario requires the larger amount of produced $\mathrm{H_2}$ due to the filling of Carriço caverns and its associated higher power losses. Hence, more $\mathrm{H_2}$ and $\mathrm{O_2}$ are sold, generating more sales. On the other hand, Scenario (D) has the lowest NPV, but still positive, for similar reasons.

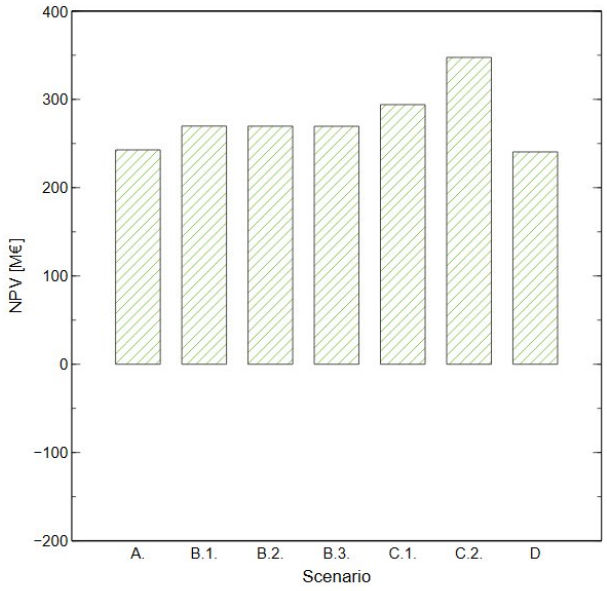

Figure 4.8: NPV [$\mathrm{M€}$] evaluated for the project of producing $\mathrm{H_2}$ to supply each scenario for transporting a mixture containing 5% of $\mathrm{H_2}$.

This scenario is where a smaller quantity of $\mathrm{H_2}$ is required due to the optimized distribution network that leads to smaller power losses. Therefore, less quantity of $\mathrm{H_2}$ needs to be produced by the electrolyser. Henceforth, there are inferior sales of $\mathrm{H_2}$ and $\mathrm{O_2}$, which decrease the project's profitability.

Sensitivity Analysis

Several sensitivity analysis are performed in the present Subsection to determine the influence of each variable on the project's NPV, for Scenario (A). The contemplated variables in the present analysis are the $\mathrm{H_2}$ selling price, electricity price, CAPEX, income tax, and industrial $\mathrm{O_2}$ selling price. The minimum and maximum considered value of each variable is presented in Table 3.5 of Section 3.2.

Firstly, the first variable to be investigated is the $\mathrm{H_2}$ selling price. The plot of Figure 4.9 exhibits the NPV as a function of the $\mathrm{H_2}$ selling price. It can be discerned that this variable strongly influences the NPV result, and the project's NPV increases when the $\mathrm{H_2}$ selling price also increases. When the $\mathrm{H_2}$ selling price decreases above 3.59 €/kg, the NPV turns negative, and consequently the project becomes economically non-viable. If the $\mathrm{H_2}$ is sold with a price higher than 3.59 €/kg, the project is always viable.

The second variable under study is the electricity price. This electricity is purchased for the electrolyser to produce $\mathrm{H_2}$. The plot of Figure 4.10 depicts the NPV as a function of the electricity price, where the NPV is observed to decrease with the increase of the electricity price. In fact, this variable also highly affects the NPV of the project. Particularly, the NPV is only positive until the electricity price reaches 0.11 €/kWh. On the other hand, if the electricity becomes more expensive than 0.11 €/kWh, the project comes to be non-viable in the economic perspective. Regardless, the near-future perspective is for the electricity price to decrease due to the expected abundant electricity from renewable sources, which improves the NPV.

The third variable to be studied in this NPV sensitivity analysis is the CAPEX. In the plot of Figure

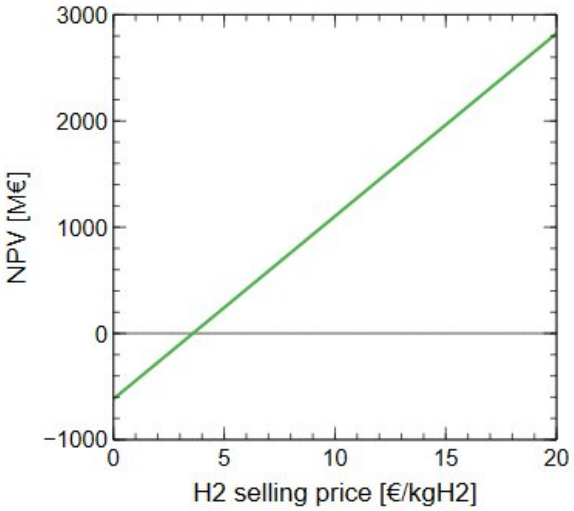

Figure 4.9: NPV [$\mathrm{M€}$] as a function of $\mathrm{H_2}$ selling price [€/kg], for Scenario (A) with 5% of $\mathrm{H_2}$.

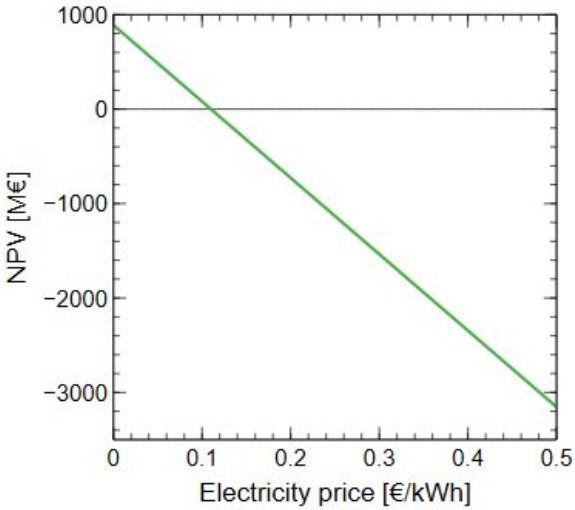

Figure 4.10: NPV [$\mathrm{M€}$] as a function of electricity price [€/kWh], for Scenario (A) with 5% of $\mathrm{H_2}$.

4.11, the NPV as a function of the CAPEX is shown. All the values within the considered range of CAPEX, presented in Table 3.5 of Subsection 3.2, culminate in a positive NPV. Therefore, the project is always economically viable for the CAPEX values considered. Subsequently, the value of the CAPEX for which the NPV becomes negative is computed, and this value is 3662.7 €/kW. This may not be problematic to turn projects into economically non-viable since the tendency is for the initial investment of the electrolysers to decrease in the future [48].

The following variable to be contemplated in the present study is the income tax rate. The plot of Figure 4.12 depicts the NPV as a function of the income tax rate, where the NPV is observed to slightly decrease with the increase of the income tax rate. As happened in the previous variable, the NPV

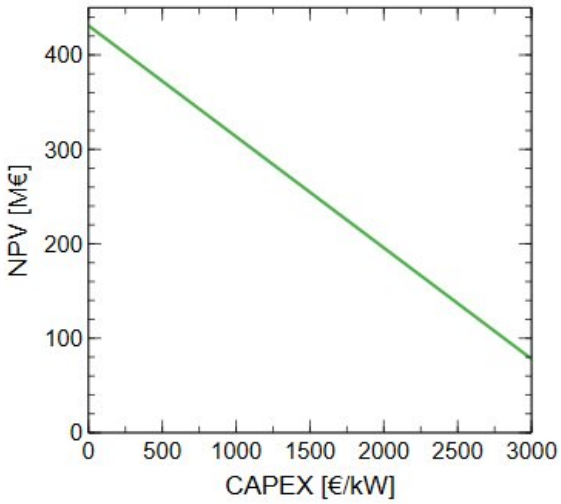

Figure 4.11: NPV [$\mathrm{M€}$] as a function of CAPEX [€/kW], for Scenario (A) with 5% of $\mathrm{H_2}$.

is always positive for the range of income tax rates considered in Table 3.5 of Section 3.2. The NPV of the project only becomes negative with an income tax rate of 72%, which is an absurd rate to be considered in the project. Therefore, the NPV is concluded to be insensitive enough to the income tax rate. Consequently, the NPV is always positive and the project is economically viable.

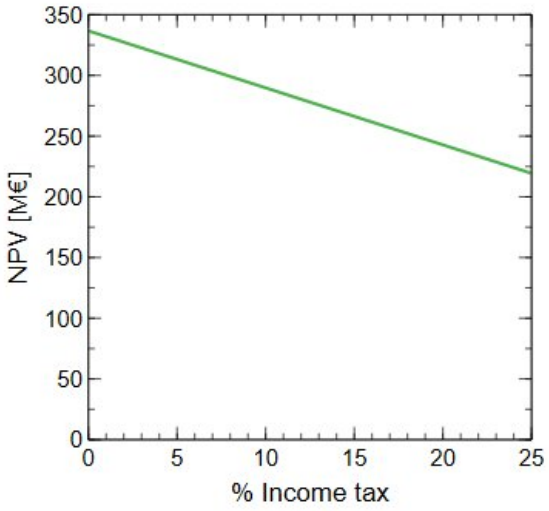

Figure 4.12: NPV [$\mathrm{M€}$] as a function of income tax rate, for Scenario (A) with 5% of $\mathrm{H_2}$.

The last variable to be accounted is the industrial $\mathrm{O_2}$ selling price. Owing to the fact that the electrolysis produces both $\mathrm{H_2}$ and $\mathrm{O_2}$, both can be sold to generate revenues. As explained in Section 3.2, the $\mathrm{O_2}$ is assumed to be sold 90% to industrial purposes and 10% to medical purposes. Therefore, the variable to be considered is the selling price of the industrial $\mathrm{O_2}$, within the range presented in Table 3.5 of Section 3.2. The plot of Figure 4.13 exhibits the project's NPV as a function of the industrial $\mathrm{O_2}$

selling price. It can be discerned that the NPV decreases when the industrial O_2 selling price increases. However, even when there are no sales, the NPV remains positive.

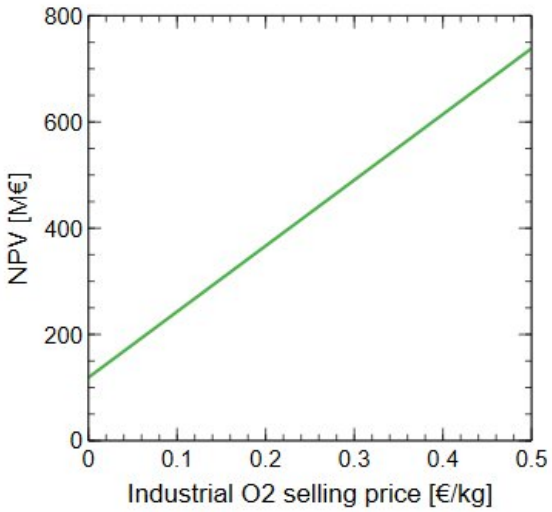

Figure 4.13: NPV [M€] as a function of industrial O_2 selling price [€/kg], for Scenario (A) with 5% of H_2.

Finally, to better understand the effect of each variable in the NPV, all of the previously considered variables are included in the plot of Figure 4.14. All the variables are varied from -100% to $+100\%$ of the respective base value. Thusly, the comparison between the influence of each variable on the project's NPV is easier, and it is simpler to make conclusions regarding which variables affect the results the most. From this combined sensitivity analysis, one can conclude that the NPV is more sensitive to the H_2 selling price and the electricity price, but with opposite effects. While the NPV sharply decreases with the increase of the electricity price, it sharply grows with the increase of the H_2 selling price. The NPV turns out negative, and the project becomes economically non-viable, when the H_2 selling price decreases to lower than 3.59 €/kg, as it is verified previously, and when the electricity prices rises over 0.11 €/kWh. When the other considered variables are varied only from -100% to $+100\%$, the project's NPV remains positive. However, it can still be concluded that the NPV is more sensitive to the CAPEX variation, followed by the industrial O_2 selling price, and finally by the income tax rate. As it is verified previously, the effect of increasing the industrial O_2 selling price on the NPV is contrary to the CAPEX and the income tax rate, since the sales of industrial O_2 are a revenue while the CAPEX and the income tax rate are expenses.

Effect of Producing Hydrogen for Several Mixture Compositions

The focus of the present study is to analyse the project's NPV of the production of H_2 for several mixture compositions to be transported to satisfy the energy demand of Scenario (A). Since this analysis just contemplates a single scenario, the only difference between the various mixture compositions relies exclusively on the quantity of produced H_2. As discerned in the study of Subsection 4.3.2, a mixture composition with a higher percentage of H_2 presents a higher power loss associated to its transmission.

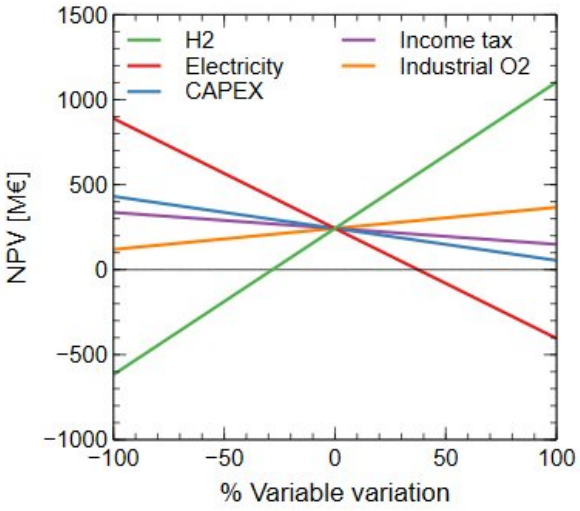

Figure 4.14: Combined sensitivity analysis of NPV [$\mathrm{M€}$] as a function of all variables being varied from -100% to $+100\%$ of the respective base value, for Scenario (A) with 5% of $\mathrm{H_2}$.

This implies that more quantity of $\mathrm{H_2}$ has to be produced in the electrolyser, to compensate both for the higher percentage of $\mathrm{H_2}$ present in the mixture as well as for the power that is lost when it is transported.

The project's NPV as a function of the percentage of $\mathrm{H_2}$ contained in the mixture that is transported to feed the energy necessities of Scenario (A) is represented in the plot of Figure 4.15. It can be observed that the trend line is not linear, which coheres with what is explained above. A larger $\mathrm{H_2}$ percentage in the mixture demands more quantity of $\mathrm{H_2}$ produced not only by the greater presence in the mixture but also due to the more considerable power losses in its transmission through the pipelines. Since more quantity of $\mathrm{H_2}$ is produced in the electrolyser, the revenue related to $\mathrm{H_2}$ and $\mathrm{O_2}$ sales is greater. Therefore, increasing the percentage of $\mathrm{H_2}$ in the mixture also increases the NPV growth rate.

4.3.4 Economic Impact on the Industry

Aside from the positive economic impact on the $\mathrm{H_2}$ producer, it is indispensable to also investigate the economic impact on industries when utilising the gas mixture composed by NG and $\mathrm{H_2}$. This analysis has the objective of studying if the industries save capital when using NG blended with various percentages of $\mathrm{H_2}$. Beforehand, it should be denoted that the attributed $\mathrm{CO_2}$ licenses will not be cost–free beyond 2030 [58]. Thus, by burning a mixture of NG with $\mathrm{H_2}$, less $\mathrm{CO_2}$ is emitted to the atmosphere, and an inferior number of licenses need to be purchased, representing a saving. However, since the price of $\mathrm{H_2}$ is higher than of NG, it should be thoroughly analysed if this change benefits or damages the industries.

One of the industries presented in the list of Appendix A.1 is selected to perform the present study. The procedure is analogous to other industries. For this study, the chosen company is a ceramic industry named C.S. Coelho da Silva. Considering a NG price of 120 €/MWh and a $\mathrm{CO_2}$ license price of 67 €/$\mathrm{ton_{CO_2}}$, as mentioned Section 3.2, the industry spends 10.81 $\mathrm{M€}$ in NG supply to feed its energy

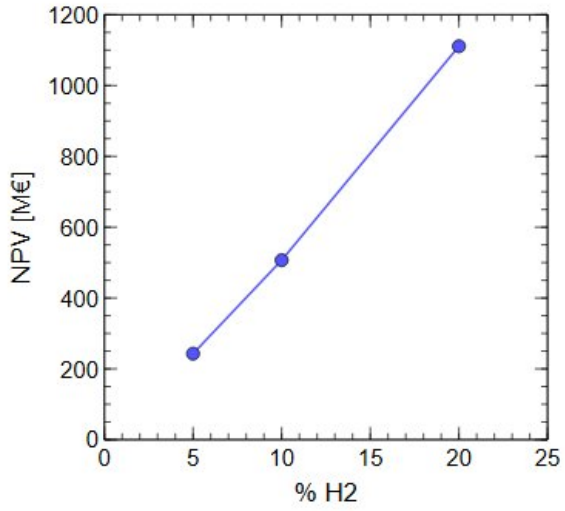

Figure 4.15: NPV [M€] as a function of the percentage of H_2 contained in the mixture that is transported to feed the energy necessities of Scenario (A).

necessities and a total 1.19 M€ related to the purchased licenses to emit CO_2. When added H_2 to the supplied gas mixture, it is assumed that no changes need to be done in the equipment and infrastructures. Therefore, the addition of this new component only involves a reduction of the number of bought CO_2 permits and purchasing the gas fuel composed by NG and H_2, with a H_2 price of 5 €/kg.

Table 4.20 shows the net licenses cost, net fuel cost, and net income, for all mixtures with several percentages of H_2. The net license cost results from the difference of the CO_2 licenses purchased for burning only NG and licenses purchased for the mixture with H_2. In fact, the usage of the new mixture composition reduces the CO_2 emissions by 1.54%, 3.19%, and 6.90%, for 5%, 10%, and 20% of H_2, respectively. The net fuel cost is obtained through the difference of cost of the fuel bought to satisfy the industry demand in the case of being only composed by NG and of being composed by NG and H_2. The net income refers to the difference between the net licenses cost and net fuel cost, as to understand if adding H_2 benefits or damages economically the industry.

Table 4.20: Net licenses cost and net fuel cost [k€] compared to the case of 100% of NG, and respective net income [k€] for each percentage of H_2.

	Net licenses cost [k€]	Net fuel cost [k€]	Net income [k€]
95% NG + 5% H_2	18.36	-41.75	-23.39
90% NG + 10% H_2	38.06	-86.65	-48.59
80% NG + 20% H_2	82.28	-187.49	-105.21

By observing the results of Table 4.20, the net licenses cost is positive for the three H_2 percentages, which holds up to the fact that there is less CO_2 being emitted to the atmosphere. Hence, the difference of cost related to CO_2 licenses represents a saving for the industries. On the other hand, the net fuel cost is negative for all mixture compositions, meaning that it is more expensive to buy the fuel with H_2 in its composition than without, since the H_2 price is higher than of NG. Therefore, this represents an

additional expense for the company. The net income is negative for the three H_2 percentages. This signifies that this fuel composition change damages the companies in the economic point of view when considering the prices assumed above.

The previous computations are effectuated considering the prices aforesaid in Section 3.2. However, this prices are extremely volatile, for example, the NG price has increased and decreased multiple times in the past few months [65]. In fact, the variation of these prices strongly affects the net income results. For this reason, the influence of each one of the three prices (NG price, H_2 price, and CO_2 license price) is analysed separately.

Firstly, the NG price is varied while the other two prices are fixed. The objective is to acknowledge the effect of the NG price on the net income. The NG price is varied from 110 €/kWh to 160 €/kWh, and the results are depicted in the plot of Figure 4.16. As expected, the NG price strongly influences the net income. For the NG prices of 110 €/kWh, 120 €/kWh, and 130 €/kWh, the net income is negative for the mixture containing 5% H_2 and it becomes even more negative when higher percentages of H_2 are blended in the fuel mixture. Since the net income is the difference between the net license cost and net fuel cost, the net income is negative when the net fuel cost is more expensive than the net license cost. This is the case for NG prices of 110 €/kWh, 120 €/kWh, and 130 €/kWh. For these lower NG prices, the net fuel cost is more expensive when adding more H_2 compared to the fixed net license costs, generating a negative net income. Besides, the definition of the net fuel cost is the difference between the cost of the fuel purchased to feed the industry demand in the case of being composed by only NG and of being composed by NG and H_2. Therefore, mixtures with higher percentages of H_2 require paying for less quantity of NG. Thus, since the NG price is lower and the H_2 is fixed, it increases the expenses for the industry when more H_2 is added. Contrastingly, the net income is positive for the mixture with 5% H_2 for the NG prices of 140 €/kWh, 150 €/kWh, and 160 €/kWh, and it increases with higher percentages of H_2. The inverse justification can be employed since the positive net income is caused by the net fuel cost being more affordable than the fixed license cost. A higher percentage of H_2 implies purchasing an inferior quantity of NG. Since the NG price is increased in the considered cases and the H_2 price is fixed, it is more affordable to buy fuel with H_2 blended compared to the net licenses cost.

The second price to be ranged is the H_2 price, considering values from 3.8 €/kg to 5.3 €/kg. Note that the NG price and CO_2 license price are fixed for this study. The plot of the net income as a function of the percentage of H_2 in the mixture, for several H_2 prices, is presented in the plot of Figure 4.17. For the H_2 prices of 5.3 €/kg, 5.0 €/kg, and 4.7 €/kg, the net income is negative for the fuel mixture with 5% H_2 and it grows more negative if a larger percentage of H_2 is blended in the mixture. This occurs due to the net fuel cost being more expensive than the fixed net license cost. The most expensive price of H_2 considered (5.3 €/kg) imply that mixtures with more percentage of H_2 have larger expenses related to the purchase of the fuel. Thus, it is more expensive to the industry to buy NG blended with H_2 than only NG. For the price of 4.7 €/kg, despite having decreased compared to base value, it is not enough to turn the net income positive. On the other hand, for H_2 prices of 4.4 €/kg, 4.1 €/kg, and 3.8 €/kg, the net income is positive and it grows even more positive with the increase of the H_2 percentage. The

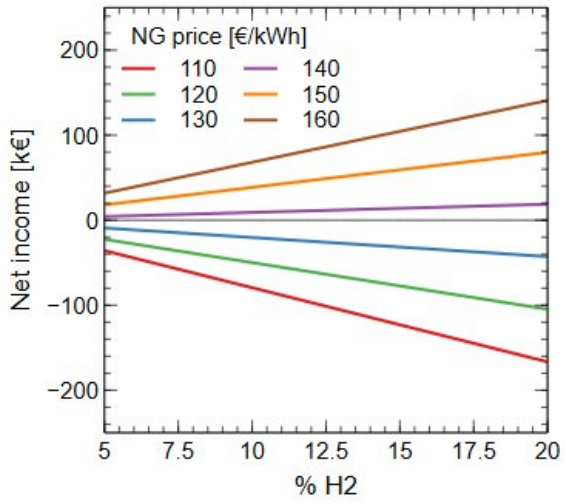

Figure 4.16: Net income [M€] as a function of the percentage of H_2 present in the mixture, for several NG prices [€/kWh].

justification for this behaviour relies on the net fuel cost being cheaper than the net licenses cost.

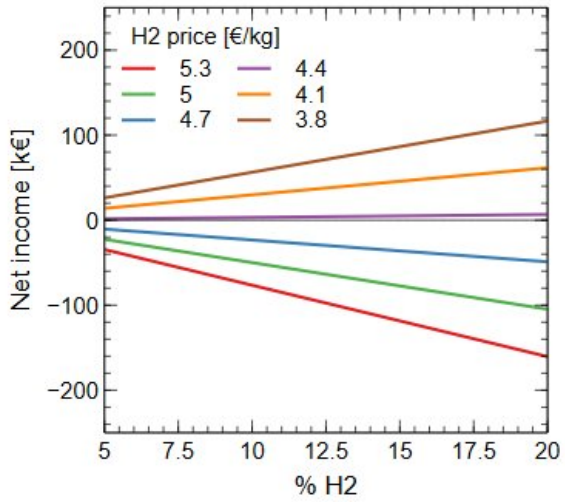

Figure 4.17: Net income [M€] as a function of the percentage of H_2 present in the mixture, for several H_2 prices [€/kg].

The last price to be varied is the CO_2 license price, while the NG and H_2 prices are fixed. A variation of the CO_2 license price between 22 €/ton and 247 €/ton is contemplated. Thereby, the results are represented in the plot of Figure 4.18. As it was acknowledged for the other prices, the net income is quite sensitive to the CO_2 license price. Particularly, the CO_2 license prices of 22 €/ton, 67 €/ton, and 112 €/ton generate a negative net income, that grows even more negative for greater percentages of H_2. The net income is negative since the net license cost is cheaper than the net fuel costs. This occurs due

to these three CO_2 licenses prices being lower causing a more positive net fuel cost. Consequently, it is economically better for the industry to continue to emit CO_2 to the atmosphere and pay for its licenses instead of purchasing more expensive fuel containing H_2. Meanwhile, if the CO_2 license prices are higher, for the cases of 157 €/ton, 202 €/ton, and 247 €/ton, the net income of adding more H_2 is positive due to being more affordable to buy fuel with more H_2, even though it is more expensive than fuel only composed by NG, than to pay higher licenses prices to emit CO_2.

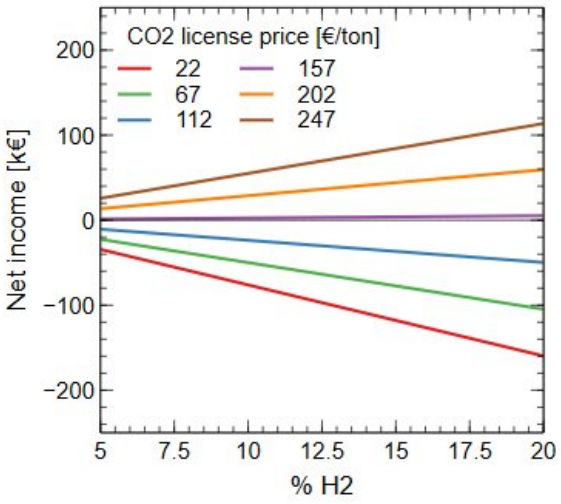

Figure 4.18: Net income [M€] as a function of the percentage of H_2 present in the mixture, for several CO_2 license prices [€/ton].

On account of the complexity to compute for what prices the industry net income is positive while fixing the remaining two, Table 4.21 briefly summarizes the values for which the net income turns positive. Therefore, for NG prices higher than 136.92 €/kWh, the net income grows positive, meaning that the change of mixture composition being delivered to the industry represents an economic benefit. For H_2 prices lower than 4.44 €/kg, the net income is also positive. Hence, with a H_2 price inferior to 4.44 €/kg, it is more advantageous to the industry this blend fuel composition. Finally, the net income also grows positive when the CO_2 license prices cost more than 152.68 €/ton. This means that purchasing fuel of the blend composition is more affordable than to pay for licenses to be entitled to emit CO_2 to the atmosphere.

Table 4.21: Prices for which the industry net income becomes positive.

	NG price [€/kWh]	H_2 price [€/kg]	CO_2 license price [€/ton]
Profit	$>$ 136.92	$<$ 4.44	$>$ 152.68

Thus, it is possible to have a positive economic impact on the industries since the CO_2 licenses are expected to become more expensive in the near-future, the H_2 price should decrease with the evolution of the electrolysis technology, and the NG price keeps becoming more expensive due to energy shortages.

Chapter 5

Conclusions

The present Dissertation was focused on the development of a computational tool that represented the gas supply to the Portuguese major industrial consumers. Several scenarios were described to characterise different supply circumstances. This computational tool determined the mass flow rate required by each industry to satisfy its energy demand and computed the power losses associated with that supply through the high-pressure network.

The developed numerical model was validated by comparing the pressure drop inside the pipeline, and a relation with the transportation efficiency was established. Afterwards, a parametric study was performed in a simplified model to acknowledge the effect of some parameters on transmission power losses. It was concluded that the percentage of power losses decreases with larger hydraulic diameter, and increases with higher mass flow rates, more extensive pipelines, and larger roughness.

Then, the results were attained for all the scenarios transporting only NG using the computational tool. The obtained power loss for Scenario (A), which involved supplying the Portuguese industrial consumers from the LNG Terminal at Sines, was 4.21%. For Scenarios (B.1), (B.2), and (B.3), which consisted of supplying the Portuguese industrial consumers from the LNG Terminal at Sines as well as exporting an extra 10% to Spain through Valença do Minho, Campo Maior, and both, respectively, their associated power losses were estimated at 5.27%, 5.23%, and 5.18%. It could be concluded that the option of exporting from both locations at the same time was the one presenting fewer power losses, therefore it was concluded to be the most interesting alternative. Scenarios (C.1) and (C.2) regarded the supply of the Portuguese industrial consumers as well as filling the caverns of Carriço Underground Storage with the maximum injection capability and doubling this capacity, respectively. The power losses were determined to be 6.00% and 7.98%. Scenario (D) used the NG stored inside the Carriço caverns to supply the Portuguese industrial consumers with the help of Sines, and the power loss was computed to be 3.22%. The conclusion was that it was advantageous to use the NG stored inside the caverns to feed the Portuguese industrial demand, however, the process of filling those caverns had its own associated power losses. Therefore, it would be beneficial to fill the caverns in periods of lower industrial consumption to reduce power losses, for example, at night. Another possibility could be building more caverns distributed along the Portuguese coast to diminish the overall power losses.

Followingly, the results were again attained for Scenario (A) but considering $\mathrm{H_2}$ present in the mixture. It was concluded that higher percentages of $\mathrm{H_2}$ in the mixture led to more power losses associated with its transmission, and they increased linearly. Linear regression was effectuated, and a correlation was developed to estimate the power losses as a function of the percentage of $\mathrm{H_2}$ contained in the mixture. This correlation could be easily modified to estimate the power losses for every scenario ($\%\text{Power losses} = 0.1295 \cdot \%\mathrm{H_2} + \mathrm{b}$).

Subsequently, an economic assessment was conducted from the perspective of the $\mathrm{H_2}$ producer to verify the economic viability of producing the $\mathrm{H_2}$ to later blend in the mixture to be transported in the RNTGN. The previously computed power losses were included in this economic study in the sense that a higher quantity $\mathrm{H_2}$ needs to be produced to compensate for the power that is lost in transmission. The determined LCOH was 4.99 €/kg, which is competitive for this type of project. The computed NPV was positive with a value of 242.79 M€, for the project of producing $\mathrm{H_2}$ necessary to supply Scenario (A) with 5% of $\mathrm{H_2}$, meaning that it is economically viable. The IRR and PBP were computed to be 21% and 5 years. The NPV was also computed for the other scenarios transporting a mixture with 5% of $\mathrm{H_2}$ and it was verified to be more profitable when a higher quantity of $\mathrm{H_2}$ is produced. Also, a sensitivity analysis was performed, and the $\mathrm{H_2}$ selling and electricity prices were the variables that affected the NPV the most.

After verifying that the project is economically viable from the perspective of the $\mathrm{H_2}$ producer, the economic analysis was conducted from the industry perspective. A specific industry was chosen to verify if the change in the supplied mixture composition had a positive or negative impact. It was concluded that the impact was negative for the prices considered, meaning that it would be more expensive to purchase the blended fuel than what would be saved in the reduction of purchased $\mathrm{CO_2}$ licenses. However, since this impact is extremely dependent on the considered prices, the economic impact of each price was studied separately. The conclusion was that, in the future, the impact may be positive since the NG price continues to increase due to energy shortages, the $\mathrm{H_2}$ prices are decreasing due to developments in electrolysis technologies, and the $\mathrm{CO_2}$ license prices are expected to become more expensive to promote further mitigation of emissions from the industrial sector.

5.1 Achievements

To summarize, the main achievements of the present Dissertation are the following:

- Creation of a computational tool in MATLAB-Simulink capable of computing the required mass flow rate to answer the energy demand of the Portuguese major industrial consumers and of determining the power losses associated to its transmission in pipelines;
- Power losses associated with the transmission decrease with larger hydraulic diameters, increase with higher entering mass flow rates, more extensive pipelines, and larger roughness;
- For the transmission of only NG in the RNTGN, supplying the industry from both Carriço and Sines has less power losses associated than just from Sines, exporting to Spain has inferior power

losses when divided through Campo Maior and Valença do Minho, and doubling Carriço injection capability has higher power losses;

- Development of a linear correlation ($\%\text{Power losses} = 0.1295 \cdot \%\text{H}_2 + \text{b}$) to predict the power losses for every scenario as a function of the percentage of H_2 present in the mixture;
- More H_2 blended into the mixture increases the power losses related to its transmission;
- LCOH of the project of producing H_2 to later be blended in the mixture is estimated to be 4.99 €/kg;
- NPV of the project of producing H_2 is positive for all scenarios, meaning that the project is economically viable, and the NPV is higher when more H_2 is produced;
- NPV is highly sensitive to the variation of the H_2 selling price and electricity price; and
- Economic impact on the industries of using NG blended with H_2 depends on the NG price, H_2 price, and CO_2 license price, and the estimation is for this impact to grow more optimistic.

5.2 Future Work

First of all, further work can be developed in analysing viable locations to build more caverns for storage, which include geographical, environmental impact, and strategic placement studies. Another research can be focused on the influence of seasonal temperature differences on the power loss results. Regarding each component of the network, more work can be performed in determining the maximum percentage of H_2 acceptable in every RNTGN component, which includes, for example, the effect of increasing the percentage of H_2 in the compressors, as well as the embrittlement in the pipelines and consequent leakage when transporting H_2. Another future study can be effectuated by considering the price of replacing components in the industries to accept the new mixture composition in economic studies.

Bibliography

[1] The Paris Agreement. https://unfccc.int/process-and-meetings/the-paris-agreement/the-paris-agreement?gclid=CjwKCAjwkaSaBhA4EiwALBgQaL4Vkvj_5ZihGN3oc_6tbzzb57hdW_rzZZD5SPUfZJ5BXUPBc2sjghoCws4QAvD_BwE. Accessed: 2022-09-15.

[2] Global Warming of 1.5 ℃. https://www.ipcc.ch/sr15/about/. Accessed: 2022-09-09.

[3] Roadmap 2050. https://www.roadmap2050.eu/. Accessed: 2022-09-09.

[4] A European Green Deal - Striving to be the first climate-neutral continent. https://ec.europa.eu/info/strategy/priorities-2019-2024/european-green-deal_en, 2019.

[5] Fit for 55. https://www.consilium.europa.eu/pt/policies/green-deal/fit-for-55-the-eu-plan-for-a-green-transition/, 2022.

[6] M. Willrich, P. Marston, D. Norell, and J. Wilcox. *Administration of energy shortages: natural gas and petroleum*. 01 1976.

[7] Run-out of the Fossil Fuels Reserves. https://ourworldindata.org/fossil-fuels. Accessed: 2022-09-10.

[8] REPowerEU: A plan to rapidly reduce dependence on Russian fossil fuels and fast forward the green transition. https://ec.europa.eu/commission/presscorner/detail/en/IP_22_3131, 2022.

[9] Y. Xie, X. Ma, H. Ning, Z. Yuan, and T. Xie. Energy efficiency evaluation of a natural gas pipeline based on an analytic hierarchy process. *Advances in Mechanical Engineering*, 9: 168781401771139, 07 2017. doi: 10.1177/1687814017711394.

[10] National Strategy for Hydrogen. https://www.dgeg.gov.pt/en/transversal-areas/international-affairs/energy-policy/national-strategy-for-hydrogen/. Accessed: 2022-10-01.

[11] J. Dudley and B. Company. BP Statistical Review of World Energy 2019. *Journal of Policy Analysis and Management*, 6:283, 01 2018.

[12] IEA - The Role of Gas in Today's Energy Transitions. https://www.iea.org/reports/the-role-of-gas-in-todays-energy-transitions, 2019.

[13] IEA - Gas 2019 Analysis and forecast to 2024. https://iea.blob.core.windows.net/assets/2c3e456a-44c2-4e7f-993e-b9f79cc2f5e9/MarketReportSeries_Gas_2019.pdf, 2019.

[14] J. Dudley and B. Company. BP Statistical Review of World Energy 2020. *Journal of Policy Analysis and Management*, 6:245, 01 2019.

[15] ERSE Caracterização da Procura de Gás Natural no Ano Gás 2020-2021. https://www.erse.pt/media/saynywdf/caracteriza%C3%A7%C3%A3o-procura-gn-2020-2021.pdf, 2020.

[16] REN – Dados Técnicos 19. https://www.ren.pt/pt-PT/media/publicacoes, 2019.

[17] Technical standards for gas – Gas Transmission Pipelines. https://www.marcogaz.org/publications/technical-standards-for-gas-gas-transmission-pipelines/. Accessed: 2022-06-08.

[18] Gas Pipeline Incidents 11th Report of the European Gas Pipeline Incident Data Group (period 1970 – 2019). https://www.egig.eu/reports, 2019.

[19] EIA - Natural gas explained: Liquefied natural gas. https://www.eia.gov/energyexplained/natural-gas/liquefied-natural-gas.php, . Accessed: 2022-04-02.

[20] Shell LNG Outlook 2022. https://www.shell.com/promos/energy-and-innovation/v1/lng-outlook-2022-report/_jcr_content.stream/1645378179742/3399fc5b65329ddf5fda80ad6cf2f6eab2abd9e5/shell-lng-outlook-2022.pdf, 2022.

[21] LNG - Terminal. https://www.ign.ren.pt/en/terminal-de-gnl3, . Accessed: 2022-03-30.

[22] X. Wang and M. Economides. Purposefully built underground natural gas storage. *Journal of Natural Gas Science and Engineering*, 9:130–137, 11 2012. doi: 10.1016/j.jngse.2012.06.003.

[23] A. Małachowska, N. Łukasik, J. Mioduska, and J. Gebicki. Hydrogen storage in geological formations—the potential of salt caverns. *Energies*, 15:5038, 07 2022. doi: 10.3390/en15145038.

[24] Hydrogen Production Processes. https://www.energy.gov/eere/fuelcells/hydrogen-production-processes. Accessed: 2022-10-10.

[25] D. Kumar and H. Vurimindi. Hydrogen production by pem water electrolysis – a review. *Materials Science for Energy Technologies*, 2:442–454, 03 2019. doi: 10.1016/j.mset.2019.03.002.

[26] J. Brauns and T. Turek. Alkaline water electrolysis powered by renewable energy: A review. *Processes*, 8:248, 02 2020. doi: 10.3390/pr8020248.

[27] F. Jurado and A. Cano. Assessing power losses in gas and electricity distribution systems. volume 2006, pages 1044 – 1047, 06 2006. doi: 10.1109/MELCON.2006.1653278.

[28] Y. Lahiouel and A. Haddad. Evaluation of energy losses in pipes. volume 5, 12 2002.

[29] E. Sletfjerding and J. Gudmundsson. Friction factor in high pressure natural gas pipelines from roughness measurements. *International Gas Research Conference Proceedings*, 01 2001.

[30] Z. Huang, Z. Chen, Q. Li, R. Zhu, S. Jing, Y. Zhou, Y. Ma, N. Wang, and W. Chang. Experimental research on the drag reduction mechanism of natural gas drag reduction agent and its industrial field test. *Industrial & Engineering Chemistry Research*, 53:12494–12501, 08 2014. doi: 10.1021/ie501478h.

[31] Y. Ma, Z. Huang, Z. Lian, W. Chang, and H. Tan. Effects of a new drag reduction agent on natural gas pipeline transportation. *Advances in Mechanical Engineering*, 11:168781401988192, 10 2019. doi: 10.1177/1687814019881923.

[32] A. Herrán González, J. de la Cruz, B. Andrés-Toro, and J. Risco-Martín. Modeling and simulation of a gas distribution pipeline network. *Applied Mathematical Modelling*, 33:1584–1600, 03 2009. doi: 10.1016/j.apm.2008.02.012.

[33] A. Woldeyohannes and M. Abd Majid. Simulation model for natural gas transmission pipeline network system. *Simulation Modelling Practice and Theory*, 19:196–212, 01 2011. doi: 10.1016/j.simpat.2010.06.006.

[34] A. Osiadacz and M. Gburzyńska. Selected mathematical models describing flow in gas pipelines. *Energies*, 15:478, 01 2022. doi: 10.3390/en15020478.

[35] Z. Hafsi, A. Ekhtiari, L. Ayed, and S. Elaoud. The linearization method for transient gas flows in pipeline systems revisited: Capabilities and limitations of the modelling approach. *Journal of Natural Gas Science and Engineering*, 101:104494, 03 2022. doi: 10.1016/j.jngse.2022.104494.

[36] M. Behbahani-Nejad and A. Bagheri. The accuracy and efficiency of a matlab-simulink library for transient flow simulation of gas pipelines and networks. *Journal of Petroleum Science and Engineering*, 70:256–265, 02 2010. doi: 10.1016/j.petrol.2009.11.018.

[37] J. Schouten, J. Michels, and R. Rosmalen. Effect of h2-injection on the thermodynamic and transportation properties of natural gas. *International Journal of Hydrogen Energy*, 29:1173–1180, 09 2004. doi: 10.1016/j.ijhydene.2003.11.003.

[38] M. Deymi-Dashtebayaz, A. Ebrahimi-Moghadam, S. Pishbin, and M. Pourramezan. Investigating the effect of hydrogen injection on natural gas thermo-physical properties with various compositions. *Energy*, 167, 11 2018. doi: 10.1016/j.energy.2018.10.186.

[39] A. Abd, S. Naji, C. Tye, and M. R. Othman. Evaluation of hydrogen concentration effect on the natural gas properties and flow performance. *International Journal of Hydrogen Energy*, 10 2020. doi: 10.1016/j.ijhydene.2020.09.141.

[40] M. Melaina, O. Sozinova, and M. Penev. Blending hydrogen into natural gas pipeline networks: A review of key issues. 01 2013.

[41] A. Witkowski, A. Rusin, M. Majkut, and K. Stolecka. Analysis of compression and transport of the methane/hydrogen mixture in existing natural gas pipelines. *International Journal of Pressure Vessels and Piping*, 166, 08 2018. doi: 10.1016/j.ijpvp.2018.08.002.

[42] C. Quarton and S. Samsatli. Should we inject hydrogen into gas grids? practicalities and whole-system value chain optimisation. *Applied Energy*, 275:115172, 10 2020. doi: 10.1016/j.apenergy.2020.115172.

[43] H. Sahin, I. Gondal, and M. Sahir. Prospects of natural gas pipeline infrastructure in hydrogen transportation. *International Journal of Energy Research*, 36, 12 2012. doi: 10.1002/er.1915.

[44] I. Gondal. Hydrogen integration in power-to-gas networks. *International Journal of Hydrogen Energy*, 44, 12 2018. doi: 10.1016/j.ijhydene.2018.11.164.

[45] J. Ogden, A. Jaffe, D. Scheitrum, Z. McDonald, and M. Miller. Natural gas as a bridge to hydrogen transportation fuel: Insights from the literature. *Energy Policy*, 115:317–329, 04 2018. doi: 10.1016/j.enpol.2017.12.049.

[46] K. Altfeld and D. Pinchbeck. Admissible hydrogen concentrations in natural gas systems. *Gas Energy*, 01 2013.

[47] Z. I. Messaoudani, F. Rigas, M. Hamid, and C. Hassan. Hazards, safety and knowledge gaps on hydrogen transmission via natural gas grid: A critical review. *International Journal of Hydrogen Energy*, 41, 08 2016. doi: 10.1016/j.ijhydene.2016.07.171.

[48] O. Schmidt, A. Gambhir, I. Staffell, A. Hawkes, J. Nelson, and S. Few. Future cost and performance of water electrolysis: An expert elicitation study. *International Journal of Hydrogen Energy*, 42: 30470–30492, 12 2017. doi: 10.1016/j.ijhydene.2017.10.045.

[49] M. Koj, J. Qian, and T. Turek. Novel alkaline water electrolysis with nickel-iron gas diffusion electrode for oxygen evolution. *International Journal of Hydrogen Energy*, 44, 10 2019. doi: 10.1016/j.ijhydene.2019.09.122.

[50] X. Wu and K. Scott. The effects of ionomer content on pem water electrolyser membrane electrode assembly performance. *International Journal of Hydrogen Energy*, 35:12029–12037, 11 2010. doi: 10.1016/j.ijhydene.2010.08.055.

[51] B. Annabelle, J. Schefold, and M. Zahid. High temperature water electrolysis in solid oxide cells. *International Journal of Hydrogen Energy*, 33:5375–5382, 10 2008. doi: 10.1016/j.ijhydene.2008.07.120.

[52] T. Nguyen, z. abdin, T. Holm, and W. Mérida. Grid-connected hydrogen production via large-scale water electrolysis. *Energy Conversion and Management*, 200:112108, 11 2019. doi: 10.1016/j.enconman.2019.112108.

[53] G. Matute, J. Yusta, and L. Correas-Usón. Techno-economic modelling of water electrolysers in the range of several mw to provide grid services while generating hydrogen for different applications: A case study in spain applied to mobility with fcevs. *International Journal of Hydrogen Energy*, 44: 17431–17442, 07 2019. doi: 10.1016/j.ijhydene.2019.05.092.

[54] G. Correa, F. Volpe, P. Marocco, P. Muñoz, T. Falagüerra, and M. Santarelli. Evaluation of levelized cost of hydrogen produced by wind electrolysis: Argentine and italian production scenarios. *Journal of Energy Storage*, 52:105014, 08 2022. doi: 10.1016/j.est.2022.105014.

[55] J.-L. Fan, P. Yu, K. Li, M. Xu, and X. Zhang. A levelized cost of hydrogen (lcoh) comparison of coal-to-hydrogen with ccs and water electrolysis powered by renewable energy in china. *Energy*, 242:123003, 12 2021. doi: 10.1016/j.energy.2021.123003.

[56] M. Minutillo, A. Perna, A. Forcina, S. Di Micco, and E. Jannelli. Analyzing the levelized cost of hydrogen in refueling stations with on-site hydrogen production via water electrolysis in the italian scenario. *International Journal of Hydrogen Energy*, 46, 12 2020. doi: 10.1016/j.ijhydene.2020.11.110.

[57] MATLAB Documentation - Simulink. `https://www.mathworks.com/help/simulink/index.html?s_tid=hc_panel`, 2019.

[58] APA - Atribuição gratuita de licenças de emissão. `https://apambiente.pt/clima/atribuicao-gratuita-de-licencas-de-emissao`. Accessed: 2022-04-26.

[59] REN – Plano de Desenvolvimento e Investimento da RNTIAT 2022-2031. `https://www.erse.pt/media/5aznhnyi/pdirg-2022-2031-mar%C3%A7o_2021.pdf`, 03 2021.

[60] W. Jia, L. Changjun, and X. Wu. Internal surface absolute roughness for large-diameter natural gas transmission pipelines. *Oil Gas European Magazine*, 40:211–213, 12 2014.

[61] The Future of Hydrogen Report prepared by the IEA for the G20, Japan Seizing today's opportunities. `https://iea.blob.core.windows.net/assets/9e3a3493-b9a6-4b7d-b499-7ca48e357561/The_Future_of_Hydrogen.pdf`, 2019.

[62] Corporate Income Tax Rates in Europe. `https://taxfoundation.org/corporate-tax-rates-europe-2019/`. Accessed: 2022-10-14.

[63] A. Keçebaş, M. Kayfeci, and M. Bayat. *Electrochemical hydrogen generation*, pages 299–317. 08 2019. ISBN 9780128148532. doi: 10.1016/B978-0-12-814853-2.00009-6.

[64] EU Carbon Permits. `https://tradingeconomics.com/commodity/carbon`. Accessed: 2022-10-17.

[65] EU Natural Gas. `https://tradingeconomics.com/commodity/eu-natural-gas`. Accessed: 2022-10-17.

Appendix A

Portuguese Industrial Consumers

This Appendix presents the list of the Portuguese CO_2-emitting industry considered in the case of study and the respective attributed CO_2 licenses. This list is adapted from [58]. The industries are placed in geographical order from Sines.

A.1 List of the Emitting Portuguese Industry and Attributed Licenses

Table A.1: List of the Portuguese CO_2-emitting industry considered in the case of study and the respective attributed licenses, adapted from [58].

Industry	Attributed CO_2 licenses
Refinaria Sines Petrogal	1507213
Repsol Polímeros	529382
Indorama Ventures	33948
Euroresinas	8141
Sutol – Indústrias Alimentares	3841
Navigator Setúbal	33
About the Future – Empresa de Papel	211524
Secil Outão	869103
AutoEuropa	2389
Lusosider Aços Planos	15414
Siderurgia do Seixal	78573
ADP Fertilizantes	16993
Central Fisigen EDP	42294
Horiticilha Agro-Indústrias	1126

Continuation in the next page

Table A.1 – *Continuation*

Industry	Attributed CO_2 licenses
Cerâmica dos Pegões	5240
FIT - Indústria do Tomate	7892
Italagro	11066
Cimpor Alhandra	1007152
Iberol S.A.	14422
ADP Fertilizantes UFAL	29450
Sociedade Central Cervejas	949
Sidul Açúcares	10758
Copam Amidos	11973
Climaespaço	3373
BA Vidro Venda Nova S.A.	46698
Sugal Group Benavente	16676
Sugal Azambuja	8952
Campil – Agro	5861
Cerâmica Toreense	8354
CT Cobert Telhas	13977
Cerâmica do Outeiro do Seixo	10618
Font Salem Portugal	1200
Lusical – Cal	279872
Calcidrata	25387
M.A Lopes d'Avó	1291
Cerâmica F. Santiago	2641
C.S. Coelho da Silva	17791
CMP Secil – Fáb. Cibra-Pataias	230470
CMP Fáb. Maceira Liz	331092
Secil Martigança	9816
Prélis Cerâmica	5984
Crisal – Cristalaria	30589
Santos Barosa Vidros	99395
Gallovidro S.A.	45453
B.A Vidros Marinha Grande	61656
Microlime – Produtos Cal	77391
Renova F1	3324
Renova F2	18056
Grestejo Cerâmicas	1792
Soladrilho	5996

Continuation in the next page

Table A.1 – *Continuation*

Industry	Attributed CO_2 licenses
Conesa Portugal	5672
Celbi	66128
Navigator Figueira Paper	196525
Navigator Figueira Pulp	4505
Cliper Cerâmica	4831
Gyptec Ibérica	4108
Celtejo – Celulose	19116
Verallia	53495
Roca	14538
Adelino Duarte da Mota S.A.	11763
Umbelino Monteiro S.A.	8595
Preceram – Indústria Construção	10218
Unigeração Lda.	9810
Leca Portugal	23232
Prado Cartolinas Lousã	5535
Cimpor Souselas	830333
CINCA Mealhada	8471
Luso Finsa – Madeiras	44718
Paulo de Oliveira S.A.	3244
Cerev Pavigrés Cerâmicas	10568
Navigator Tissue Vila Velha Rodão	11543
Paper Prime S.A.	8171
Sanitana Anadia	15268
Pavigrés Sede	15932
Pavigrés Grespor	9158
Cerdomus	3778
Modicer – Moda Cerâmica	4972
Gresart	11170
Solcer	5120
Recer	10610
CETIPAL	2927
Preceram Norte	5737
Revigrés	10866
Sociedade Cerâmica do Alto	4071
Inacer	3630
Argex	11583

Continuation in the next page

Table A.1 – *Continuation*

Industry	Attributed CO_2 licenses
Pavigrés II Bustos	2232
Sanindusa	6359
Tijolágueda	2709
Cerâmica das Quintãs	5440
Gres Panaria	13597
Primus Vitória – Azulejos	4521
Ria Stone	6892
Bresfor	12054
Love Tiles	19121
Navigator Aveiro	30044
Bondalti Chemicals	50283
Dow Portugal	44396
Fáb. PVC Cires	12654
Sociedade Portuguesa Ar Líquido	38700
Fáb. Papel da Lapa	2626
Papelaria Coreboard	9335
Fábrica Zarrinha	3939
Oliveira Santos e Irmão	2588
Cinca Fiães	10777
Sociedade Transformadora Papel Vouga	2110
B.A Glass Avintes	68766
RAR – Cogeração	15189
Unicer – Energia e Ambiente	1912
Refinaria Porto	395260
Companhia Térmica Tagol	29296
Sn Maia – Siderurgia Nacional	54606
Termolan isolamentos	9036
Riopele Têxteis	7759
F.S. Cerâmica Amaro e Macedo	6284
dst – Domingos de Silva Teixeira	1027
Fortissue	6135
Europac Kraft Viana	98238
Mgc – Acabamentos Têxteis	8221

End